EFFECT OF ZNO MORPHOLOGY ON PHOTOCATALYTIC ACTIVITY
DETERMINED BY NO OXIDATION

A THESIS SUBMITTED TO
THE GRADUATE SCHOOL OF NATURAL AND APPLIED SCIENCES
OF
MIDDLE EAST TECHNICAL UNIVERSITY

BY

ORHUN KAHRAMAN

IN PARTIAL FULFILLMENT OF THE REQUIREMENTS
FOR
THE DEGREE OF MASTER OF SCIENCE
IN
CHEMICAL ENGINEERING

APRIL 2019

Approval of the thesis:

EFFECT OF ZNO MORPHOLOGY ON PHOTOCATALYTIC ACTIVITY DETERMINED BY NO OXIDATION

submitted by **ORHUN KAHRAMAN** in partial fulfillment of the requirements for the degree of **Master of Science in Chemical Engineering Department, Middle East Technical University** by,

Prof. Dr. Halil Kalıpçılar
Dean, Graduate School of **Natural and Applied Sciences**   _____

Prof. Dr. Pınar Çalık
Head of Department, **Chemical Engineering**   _____

Prof. Dr. Deniz Üner
Supervisor, **Chemical Engineering, METU**   _____

Assist. Prof. Dr. Ertuğrul Erkoç
Co-Supervisor, **Chemical Eng. Dept., Bursa Tech. Uni.**   _____

Examining Committee Members:

Assist. Prof. Dr. Harun Koku
Chemical Engineering Dept., METU   _____

Prof. Dr. Deniz Üner
Chemical Engineering, METU   _____

Assist. Prof. Dr. Ertuğrul Erkoç
Chemical Engineering Dept., Bursa Technical University   _____

Assoc. Prof. Dr. Dilek Duranoğlu Dinçer
Chemical Engineering Dept., Yıldız Technical University   _____

Assist. Prof. Dr. Bahar İpek
Chemical Engineering Dept., METU   _____

Date: 29.04.2019

I hereby declare that all information in this document has been obtained and presented in accordance with academic rules and ethical conduct. I also declare that, as required by these rules and conduct, I have fully cited and referenced all material and results that are not original to this work.

Name, Surname: Orhun Kahraman

Signature:

ABSTRACT

EFFECT OF ZNO MORPHOLOGY ON PHOTOCATALYTIC ACTIVITY DETERMINED BY NO OXIDATION

Kahraman, Orhun
Master of Science, Chemical Engineering
Supervisor: Prof. Dr. Deniz Üner
Co-Supervisor: Assist. Prof. Dr. Ertuğrul Erkoç

April 2019, 85 pages

In this thesis, the ISO 22197-1 standard test method -for assessing photocatalytic activity by NO oxidation- was used to determine the activity of a series of ZnO samples prepared by a wet chemical synthesis method. The crystallinity of the samples was monitored by XRD and the morphology of the samples was investigated by SEM analysis. NO oxidation measurements revealed that the samples having long range ordered hexagonal morphology shown better photocatalytic activity than those with flake-like morphology. Further analysis suggested that the 001 plane of wurtzite is the most active plane for photocatalytic NO oxidation.

.

Keywords: ZnO, Morphology, Photocatalysis, NO Oxidation

ÖZ

ZNO MORFOLOJİSİNİN NO OKSİDASYONU İLE BELİRLENEN FOTOKATALİTİK AKTİVİTE ÜZERİNE ETKİSİ

Kahraman, Orhun
Yüksek Lisans, Kimya Mühendisliği
Tez Danışmanı: Prof. Dr. Deniz Üner
Ortak Tez Danışmanı: Dr. Öğr. Üyesi Ertuğrul Erkoç

Bu tez çalışmasında, NO oksidasyonu ile fotokatalitik aktiviteyi değerlendirmek için kullanılan ISO 22197-1 standart test metodu, ıslak kimyasal sentez metodu ile hazırlanan bir dizi ZnO numunesinin aktivitesini belirlemek için kullanılmıştır. Numunelerin kristal yapıları XRD yöntemi ile incelendi ve numunelerin morfolojisi SEM analizleri ile gözlemlendi. NO oksidasyon ölçümleri, wurtzite yapısının altıgen morfolojisine sahip numunelerin pul benzeri morfolojisine sahip olanlardan daha iyi performans gösterdiğini ortaya koymuştur. Yapılan analizler 001 wurtzite düzleminin fotokatalitik NO oksidasyonu için en aktif düzlem olduğunu ortaya koydu..

To My Family

ACKNOWLEDGEMENTS

TABLE OF CONTENTS

LIST OF TABLES

TABLES

LIST OF FIGURES

FIGURES

LIST OF ABBREVIATIONS

ABBREVIATIONS

BET	Brunauer- Emmett-Teller
CB	Conduction Band
CSTR	Continuous stirred-tank reactor
F_{NO}	NO Molar Flowrate
ISO	International Organization for Standardization
MFC	Mass Flow Controller
PFR	Plug Flow Reactor
PM	Particulate Matter
r_{NO}	Rate of NO Oxidation
RTD	Residence Time Distribution
SEM	Scanning Electron Microscope
UV	Ultraviolet
VB	Valence Band
XRD	X-ray Diffraction

CHAPTER 1

INTRODUCTION

1.1. Photocatalytic NO Oxidation Reaction

Continuous growth of industries and the constant increase of energy demand cause steady increase of hazardous gas emissions in the atmosphere. Those toxic components pose a threat for the human life by accelerating the health issues across the World. Because of this, the air quality research became one of the most important challenges for the human kind. Along with particulate matter (PM), gases such as ozone (O_3), carbon monoxide (CO), sulfur dioxide (SO_2) as well as Nitrogen Oxides (collectively named as NOx) are the common hazardous species present in the atmosphere[1].

Currently, the rate of emission of pollutant gases is higher than its natural removal by the soil and water. Therefore, utilizing artificial ways of abatement techniques are necessary to decrease the environmental issues caused by the pollutant gases[2]. NOx is one kind of the air pollutant gases which is mainly emitted by the combustion processes and it is composed of largely NO and to a small extent of NO_2. It is not only known as the source of photochemical smog and acid rain, but an important factor for health problems associated with cardiovascular and respiratory systems[2].

While different techniques for NOx abatement are being developed, heterogeneous photocatalytic oxidation is one of the most promising approaches that is being studied across the globe where metal oxide semiconductors are mostly being utilized. Photocatalytic NO Oxidation reaction is mainly initiated with the absorption of photon energy with equal or higher than the band gap of the semiconductor material, which leads to generation of electron hole pairs followed by the separation of charges [3].

The rest of the mechanism can be explained with classical catalysis phenomenon. Various different redox reactions take place with the generated electron and hole pair once they reach to the catalyst surface, where the NO photo oxidation reaction is one of them [4].

$$MOx + hv \rightarrow MOx\ (h^+_{vb} + e^-_{cb}) \qquad (1.1)$$
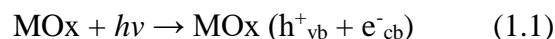
Photocatalytic self-cleaning surfaces has already been used in some real scale applications in several countries where the streets are treated with photocatalyst materials [5]. Concrete is commonly used in buildings and streets, making them closely related to our lives. Thus, turning concrete into an eco-friendly material to reduce NOx is an attractive research area[6]. Mainly, the concrete structures blended with photocatalytic materials are being studied and this research is getting more popular especially in the European countries [6], [7].

Table 1: Some examples of TiO$_2$ containing paved surfaces in the World [8]

Located City	Installed Place	Pavement Surface Area (m^2)	Type of Pavement	Ref.
Antwerp, Belgium	Parking lanes of urban road	10000	Paving blocks	[9]
Via, Morandi, Segrate	Urban road	7000	Thin mortar overlay	[10]
Bergamo, Italy	Industrial site road	80000	Paving blocks	[11]
Vanves, Paris, France	Urban road	250 m lenght	Thin bonden concrete overlay	[12]
Wijnegem, Belgium	Industrial Site Road		Concrete, two-lift construction	[13]
Baton Rouge, Los Angeles, US	Urban Road		Spray coating on concrete	[14]
Multiple Locations, Japan	Sidewalks and urban roads	25000	Paving blocks	[15]
Milan, Italy	Parking Garage	4000	Spray coating on asphalt	[16]

Hengelo, Netherlands	Urban Road	750-1200	Paving blocks	[2]
Copenhagen, Denmark	Urban Road		Paving blocks	[17]

(*Table 1 continued)

1.2. ZnO Photocatalysis

Several semiconductor oxide materials are being reported in the literature for their use photocatalytic properties and potential applications. Some of the most commonly studied oxides are TiO_2, SnO_2, CeO_2 and ZnO [18]. Although the major research is based on TiO_2 and it has already been used in several applications, ZnO is another good candidate for photocatalytic applications due to its high photosensitivity, appropriate redox potential, high natural abundance, non-toxicity and its relatively low cost [19]. Besides, ZnO can be synthesized by a great variety of morphologies depending on the synthesis route that is followed[20].

ZnO is a competitive alternative for TiO_2 and a promising substance for environmental applications. It has a wide band gap energy in the near-UV spectral region which is very close to the band gap of TiO_2; thus, similar photocatalytic efficiency is expected with TiO_2 [21]. In fact, since a larger fraction of the solar spectrum is absorbed by ZnO surface, it is reported as having higher light absorption efficiency compared to TiO_2, which is the major advantage of ZnO over TiO_2 for photocatalytic applications especially under sunlight [22]. Besides, ZnO is easier to produce and a cheaper alternative of TiO_2, making it suitable for large scale applications in comparison to TiO_2[21]. In addition to this, having a large free exciton binding energy enables ZnO to perform excitonic emission processes even at temperatures above the room temperature[23]. Moreover, ZnO is compatible with living organisms, making it suitable for consumer products and applications.

Several different synthesis methods are available for the fabrication of ZnO with characteristic morphologies. These methods include precipitation, solvothermal, sol-

3

gel, wet chemical synthesis method and many others. Through these methods, the morphology can be controlled by changing variables during the synthesis such as reaction time, addition of moderators, chelating agents and other auxiliary reagents[24].

In the literature, there are several studies revealing that different ZnO surface morphologies favor characteristic photocatalytic activity [25]. According to them, difference in morphology brings variation in surface atomic arrangements, different specific surface area, change in the light absorption properties, different electron-hole recombination and charge separation kinetics and many other properties. In other words, morphology has a key role in the photocatalysis research leading to variation in the photocatalytic activity[26]. Thus, establishing a control over the morphology is an important challenge in the photocatalysis with ZnO structures.

1.3. ISO 22197:2007 (E) Standard Experiment

This ISO certified method specifies an experimental procedure for determination of air-purification performance of photocatalytic materials. Mainly metal oxide semiconductor materials such as TiO_2, ZnO, CdS or other ceramic type materials are being examined in this standard experiment. The set-up is based on continuous exposure of the given air pollutant gas (NOx) to the coated test piece to under the illumination of UV light. The NOx removal rate is continuously monitored through a NOx analyzer working with chemiluminescence principle [27]. The standard contains a detailed description of required apparatus and procedures to have accurate results. Nevertheless, this method is only applied to examine the photocatalytic materials for air purification purposes. Thus, it is not recommended to test the materials for self-cleaning, antifogging, antibacterial or water contamination performances by the standard [27].

4

Considering that the study of pollutant gas removal with photocatalytic routes is becoming a popular challenge among the environmental catalysis research, there is now a strong need to quantify the photocatalytic performance of the materials with high accuracy. Regarding this issue, NO oxidation method is a good candidate to determine the photocatalytic activity of semiconductor oxides at mild conditions with high accuracy unlike the traditional organic dye degradation methods [28].

1.4. Objectives of the Thesis

The objective of this research is to use an experimental set-up that complies with the procedures and requirements of ISO-22197 air purification test standard to quantify photocatalytic activity of different surfaces and perform comparison with the other materials.

ZnO structures labeled AT-1 to AT-19 with various morphologies were synthesized by Admire Tech with 7 different ZnAc:NaOH ratios under different flow regimes. XRD, SEM and BET characterization techniques were conducted to analyze ZnO structure and their photocatalytic activities were quantified with the NO oxidation reaction to find relationship between the morphology and the photocatalytic performance.

CHAPTER 2

LITERATURE SURVEY

2.1. Heterogeneous Photocatalysis

Over the past four decades, heterogeneous photocatalysis became a widespread research topic across the globe due to its versatile application areas such as gaseous pollutant removal, water detoxification, artificial photosynthesis, production of solar fuels, and many others [29]. Although the first applications of photocatalysis have been studied in early 20th century, after the discovery of photoelectrochemical decomposition of water by Fujishima and Honda in 1972, a significant attention is devoted to this area [30]. The first applications of heterogeneous photocatalysis was mainly related to hydrogen production technology. The reason of this can be associated with the oil crisis which was taken place at a very close time to this discovery. However, it was after realized that the TiO_2 absorption of light was limited with around 3% of UV in the solar spectrum, so interest of hydrogen production using heterogeneous photocatalytic approaches gradually depleted. Instead, the research shifted to destruction of pollutants [30]. Soon after several other applications including photocatalytic pollutant gas abatement and detoxication of harmful components in water drew significant attention as the environmental problems are getting more and more serious across the globe. The first studies concerning the oxidization of harmful components released by Frank and Bard in 1977 addressing the issue of cyanide decomposition in water [31]. Thereafter several detoxication studies were demonstrated concerning both air and water using TiO_2 in the powder form showing a strong candidate for air and water purification methods. Many reviews then have been published in the early 90's such as Bahnemann [32] and Fox [33] summing up

the terms in heterogeneous photocatalysis for environmental detoxifications mainly within the scope of TiO_2 surface phenomena.

Semiconductor materials with a certain band gap energy are mainly used for the applications of heterogeneous photocatalysis [34]. Basically, the photons from the light source create the so-called electron hole pairs that can later perform chemical work such as photooxidation for reducing of some compounds. Different light sources can be used for this process but the most reasonable light source is the readily available sunlight [34].

Relatively wide band gap materials such as TiO_2 and ZnO favor suitable redox potential with high stability. Nevertheless, their absorption of light is limited to UV spectrum due to their relatively larger band gap of 3-3.2 eV. Thus, a vast amount of research is devoted on increasing the absorption spectrum as well as finding new possible photocatalysts materials such as the perovskite structures [35].
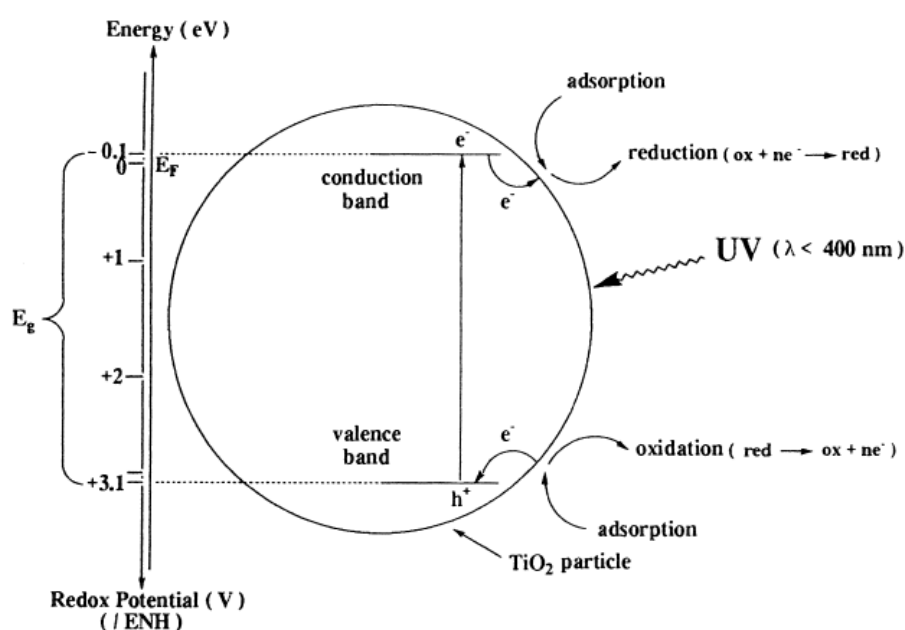
Figure 1: Energy band diagram of titania adapted from [34] with permission

8

Understanding the mechanism of photocatalytic reactions is important to develop and design new photocatalytic materials. The principle of the heterogeneous photocatalysis is very similar to classical catalysis except for the initiation of the surface with the absorption of light and generation of electron hole pairs, unlike the thermal activation in the classical catalysis [34]. In other words, once the semiconductor surface is exposed to light energy followed by the generation of electron-hole pairs, the reaction mechanism is proceeded as; adsorption of the reactants to the catalyst surface, reaction of the reactants in the adsorbed phase followed by the desorption and removal of the products [34].

By the mid 90's there has been a well established understanding of photochemical processes on semiconductor surfaces upon irradiation [33]. The absorption of photon energy in the surface and the generation of electron hole pairs have profound importance in the process and this concept is explained in detail by Fox within the scope of electron band theory [33].

The incoming light with the energy higher or equal to the band gap of the semiconductor can succeed in transferring one electron from the valance band to the conduction band. Creating an electronic vacancy or "hole" (h^+) at the valance band edge and producing photoexcited electrons (e^-) in the conduction band [30]. Due to lack of continuum of the interband states, semiconductors have relatively lower rates of recombination of this electron hole pair, unlike metals [33]. Fortunately, this helps to sustain sufficient lifetime for the electron-hole pair to participate various electron transfer reactions [33].

The so-called electron hole pair is capable of performing interfacial electron transfer reactions upon surface-adsorbed species. Nevertheless, for the reaction to take place, it is first compulsory for the generated charges to be transferred across the surface interface. In addition to that the adsorbed species must have a suitable redox potential with the catalyst material to satisfy the thermodynamics of the reaction [36].

Once the photogenerated charges reach to the the catalyst surface, an adsorbed electron donor can be oxidized by the hole to become a cation radical $D\bullet^+$, while an adsorbed electron acceptor can be reduced by the electron at the surface to become an anion radical $A\bullet^-$ [33]. For the case of water adsorption on the semiconductor surface, once the electron and holes reach to the surface, holes react with adsorbed water to form hydroxyl radicals, and electrons react with the oxygen molecules to form superoxide radicals, where both species are highly reactive and capable of oxidizing NO molecules [37].

$$SC + h\nu \rightarrow (e^-, h^+) \tag{2.1}$$

$$h^+ + D \text{ (adsorbed)} \rightarrow D\bullet^+ \text{ (adsorbed)} \tag{2.2}$$

$$e^- + A \text{ (adsorbed)} \rightarrow A\bullet^- \text{ (adsorbed)} \tag{2.3}$$

Finally, the photoinduced reduction reaction can take place if the bottom of the conduction band is more negative than the reduction potential of the adsorbed molecule. Similarly, for the photoinduced oxidation reaction to take place, the top of the valence band must be more positive than the oxidation potential of adsorbed substrate molecule. So that the thermodynamics of the redox reactions are satisfied.

10
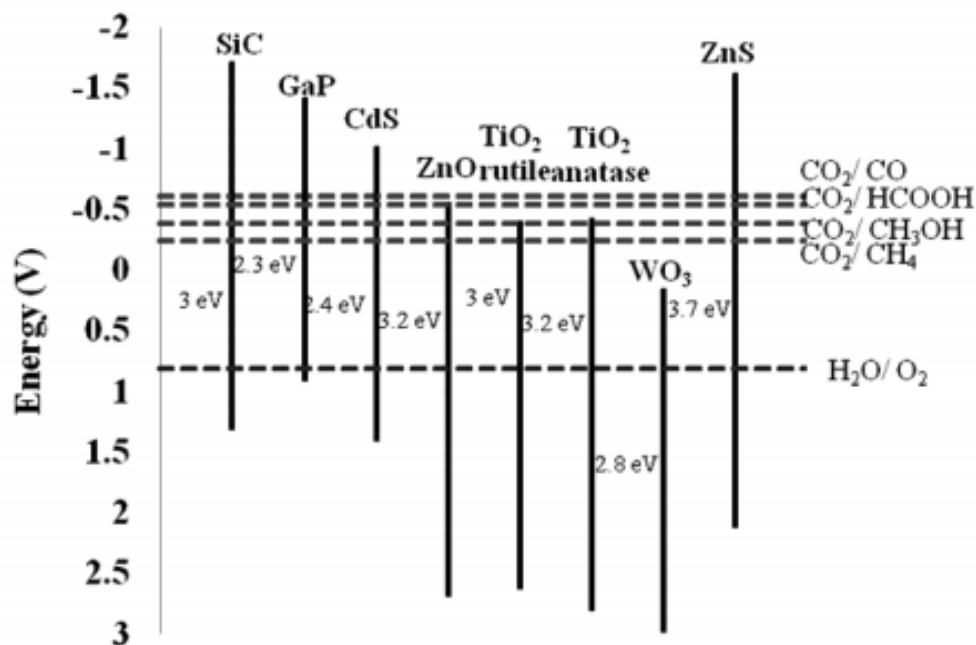
Figure 2: Band levels of several semiconductor materials and redox couples (eV vs. NHE at pH = 7) adapted from [38] with permission

The band gap of the semiconductor is one crucial factor that determines the absorption wavelength range to create electron – hole pairs. But, a suitable redox potential is also necessary to transfer the photoinduced electrons to adsorbed species and perform the desired oxidation and reduction reactions [39]. The main reasons why TiO_2 is the most commercially used semiconductor is not only because of its reasonable production cost, good chemical stability and low toxicity, but also its diversity in number of different possible redox reactions [40]. The band gap of some selected semiconductors and their corresponding VB and CB levels are deployed in Table 2.

11

Table 2: Some semiconductors and their corresponding VB and CB levels [39]

Semiconductor	Band level with respect to NHE (eV)		
	CB	**VB**	**Eg**
ZrO_2	-0.75	4.25	5.0
Ta_2O_5	-0.06	3.94	4.0
ZnS	-0.91	2.44	3.35
$KTaO_3$	-0.48	3.02	3.5
GaN	-0.5	3.0	3.5
$SrTiO_3$	-0.81	2.59	3.4
TiO_2 (Anatase)	-0.25	2.95	3.2
TiO_2 (Rutile)	-0.05	2.95	3.0
In_2O_3	-0.17	2.63	2.8
SiC	-0.46	2.34	2.8
CdSe	-0.54	1.16	1.7
GaP	-0.97	1.23	2.2
CdS	-0.52	1.88	2.4
SnO_2	0.19	3.69	3.5
NiO	0.05	3.55	3.5
$BaTiO_3$	0.55	3.85	3.3
ZnO	0.15	3.35	3.2
$CuTiO_3$	0.19	3.18	3.0
$FeTiO_3$	0.1	2.9	2.8
WO_3	0.71	3.41	2.7
$CdFe_2O_4$	0.55	2.85	2.3
Fe_2O_3	0.73	2.93	2.2
CdO	0.74	2.94	2.2
Cu_2O	0.16	2.36	2.2
CuO	-0.96	2.66	1.7
MoS_2	0.23	1.4	1.2

In conclusion the photocatalytic reactions on semiconductor surfaces can be generalized with the following five steps [36]

a. Absorption of light and creation of electron-hole pairs

b. Charge separation of the formed electron-hole pairs to the semiconductor surface

c. Formation of hydroxyl radicals and superoxide ions via redox reactions

d. Photodecomposition of surface pollutants via reaction with active species on the semiconductor surface.

e. Desorption of the products from the surface interface.

The redox potential levels of the adsorbed species and valence band and conduction band edge positions of the semiconductor material highly determines the probability and the charge transfer rate processes for the generated electron and holes. Another possibility for the process to proceed after the electron hole generation is the recombination which is the back-donation of the charges. Recombination is a big issue in the photocatalysis upon semiconductor surfaces as it decreases the quantum yield of the process which is defined as the number of events occurring per photon absorbed in the system [41].

To decrease the recombination rate and thus increase the quantum yield of the process there are several surface modification methods available such as addition of metals and dopants, surface sensitization or coupling the surface with another semiconductor material [34]. Also, the rate of recombination will differ at particularly different morphologies which is the case in ZnO where several morphologies can be obtained easily depending on the method of crystal growth and synthesis conditions [42]. Those methods also assist the process to take place in the visible light spectrum, which is just another challenge in the heterogeneous photocatalysis.

2.2. ZnO Structure and ZnO Photocatalysis

ZnO is a group II-VI semiconductor material with unique chemical and physical properties such as, high photostability, low toxicity, good radiation absorption, high chemical stability and many others [43]. It has a wide range of applications from catalysis to electronics. ZnO has a large direct band gap of ~3.37 eV at room temperature and a large excitation binding energy of 60 meV which makes it suitable

for applications in electronics, optoelectronics and laser technology[43]. Its low toxicity and biocompatibility makes it possible for use in biomedical applications [24]. Also, due to its rigidity, hardness and piezoelectric constant, it has various applications in the ceramic industry [24]. The photocatalytic activity of ZnO is comparible with that of TiO_2 considering the similarity in their band gaps and their corresponding energetic locations of VB and CB [44]. In addition to that the production cost of ZnO is 75% lower than the production cost of Al_2O_3 and TiO_2 as it is indicated by Liang et al [45].

ZnO has tetrahedral bonding configuration and it can be crystallized in three different polymorphs, which are cubic rocksalt, cubic zinc blend or hexagonal wurtzite structures. Only at very high pressures ZnO can stabilize in rocksalt structure, while zincblende can be formed by growing ZnO on cubic substrates only [46]. On the other hand, hexagonal wurtzite structure is the most thermodynamically favored polymorph under normal working conditions [47].

(a)   (b)   (c)
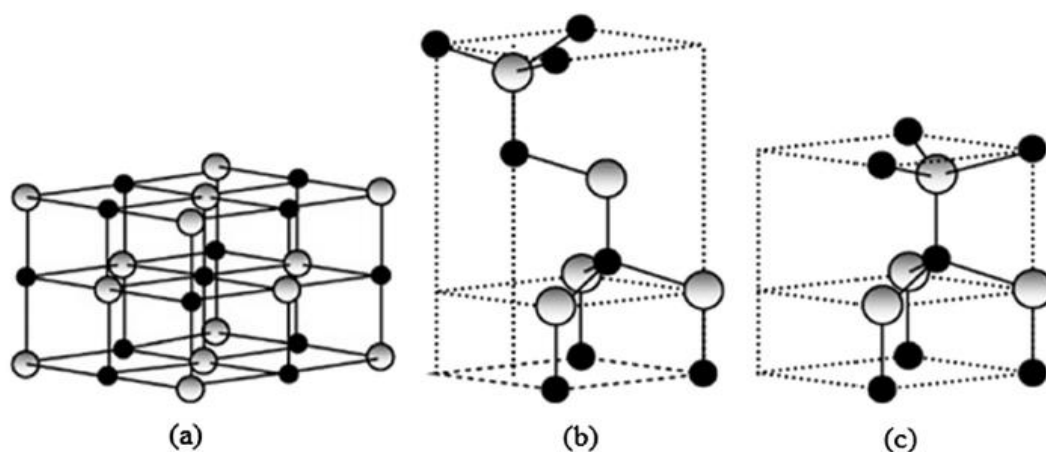
Figure 3: ZnO polimorphs a) cubic rocksalt structure b) cubic zinc blende structure c) hexagonal wurtzite structure adapted from [48] with permission

14

For the wurtzite structure, each ion is surrounded by a tetrahedron of four counterions i.e. both ions are (4,4) coordinated. Because of the tetrahedral coordination of both Zn^{+2} and O^{-2} ions, there appears a noncentral symmetric structure which eventually gives the pyroelectric and piezoelectric properties of ZnO [49].

ZnO makes a good candidate for photocatalytic applications due to several reasons. Firstly, large band gap provides an excellent driving force to induce redox reactions with relatively less recombination rates. In addition, it has high photosensitivity and relatively non-toxic, which are strong assets in photocatalytic applications. There are plenty of different techniques to synthesize ZnO structures with various different morphologies, even possible with different starting materials. Moreover, it has high solubility in various solvents and it has high abundance in nature [19]. All of these traits apparently make ZnO a good alternative for TiO_2 in photocatalytic applications. In fact, according to some studies in the literature, ZnO exhibits a better efficiency than commercial titania for the generation of photoactive species [50]–[52]. Nevertheless, ZnO is not a perfect material for photocatalytic applications. It has several drawbacks, which are open for further improvements. First of all, due to its wide band gap, visible light is not sufficient to perform the photo excitation and creation of electron hole pair; instead, UV light is necessary for photo excitation which is present at only 2-5% of the solar spectrum [19]. The rapid recombination rate of the charge carriers is another major issue to be improved at ZnO structures since it lowers down the quantum yield. Moreover, under UV light there is a tendency to aggregate during the catalytic reactions results in photo dissolution of ZnO through the so-called pitting corrosion effect [53]. Thus, utilization of visible light and finding solutions to the rapid recombination are two of the major concerns in ZnO photocatalysis.

Although the major photocatalysis research is based on TiO_2, the research on ZnO for photocatalysis had a significant boost since the beginning of century. As it is indicated in Figure 4 there is an exponential increase in the number of papers published with ZnO as photocatalyst and research with the ZnO doped photocatalyst materials [54].

The main mechanism of ZnO photocatalysis is very similar to that of the one with TiO$_2$. The photogenerated electron-hole pairs migrate to the surface and perform the redox reactions. In the solution phase, the so called hole (h$^+$) reacts with the hydroxide ion and adsorbed water molecule to give hydroxyl radicals, while photogenerated electron (e$^-$) reacts with oxygen to give superoxide radical anion followed by hydrogen peroxide [55]. Finally, the superoxide radicals proceed with another reaction, this time with the hydrogen peroxide to yield hydroxyl radicals, which are strong oxidizing agents. Once the hydroxyl radicals are generated, the reaction mechanism can proceed according to the adsorbed substrate [56]. The generation of hydroxyl radicals are given below from equation (2.4) to equation (2.12) according to the mechanism proposed by Shanti et al. [56]:

$$ZnO + hv \rightarrow (e^-_{CB}) + (h^+_{VB}) \tag{2.4}$$

$$(h^+_{VB}) + H_2O \rightarrow ZnO + H^+ + OH\bullet \tag{2.5}$$

$$(h^+_{VB}) + OH^- \rightarrow ZnO + OH\bullet \tag{2.6}$$

$$(e^-_{CB}) + O_2 \rightarrow ZnO + O_2\bullet^- \tag{2.7}$$

$$O_2\bullet^- + H^+ \rightarrow HO_2\bullet \tag{2.8}$$

$$HO_2\bullet + HO_2\bullet \rightarrow H_2O_2 + O_2 \tag{2.9}$$

$$(e^-_{CB}) + H_2O_2 \rightarrow OH\bullet + OH^- \tag{2.10}$$

$$H_2O_2 + O_2\bullet^- \rightarrow OH\bullet + OH^- + O_2 \tag{2.11}$$

$$H_2O_2 + hv \rightarrow 2\ OH\bullet \tag{2.12}$$
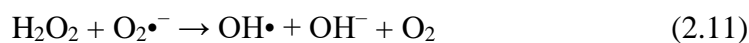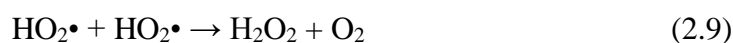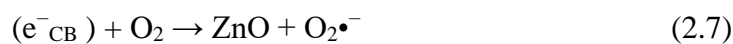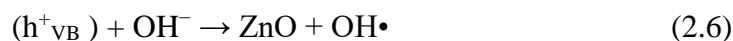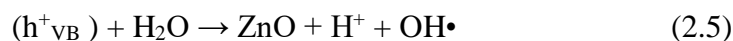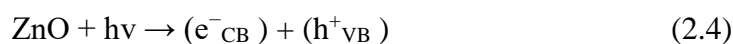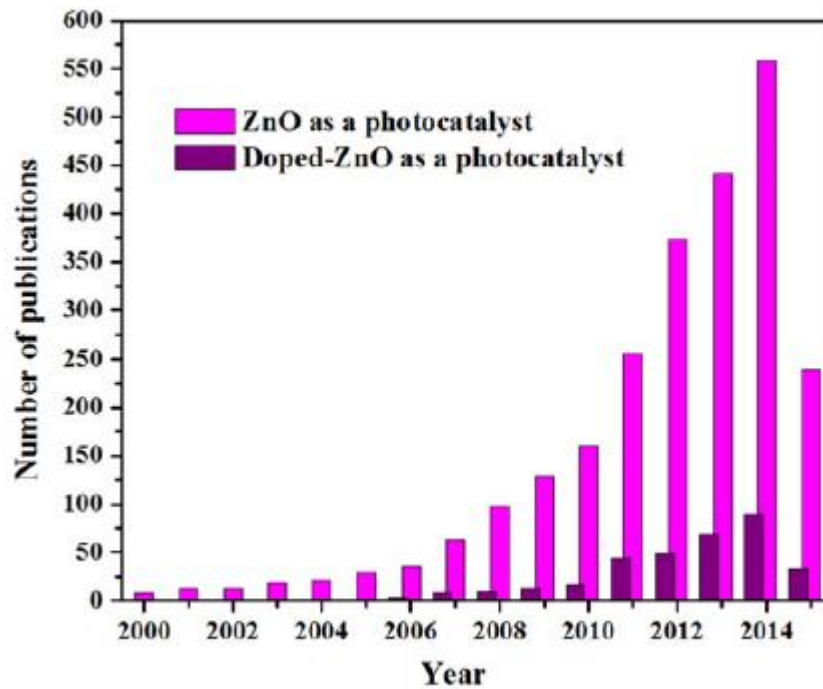
Figure 4: Number of publications based on ZnO and ZnO doped photocatalysis studies from January 2000 to May 2015 adapted from [54] with permission

Recently several research papers revealed that there is in fact a strong relationship between morphology of the ZnO structure and its photocatalytic activity[57]–[59]. According to them, the charge separation properties and the band gap energies of semiconductors are strongly dependent on crystallinity, size and the crystal phase. Thus, the idea of increasing photocatalytic efficiency by finding the most appropriate fabrication method to achieve a certain morphology is a recent topic in ZnO photocatalysis [60]. The photocatalytic activity can be improved by changing surface lattice plane and the surface area of the crystal. Thus, an appropriate geometric structure can influence the carrier transfer pathways resulting in improving in photocatalytic activity [19]. Understanding and modifying the fabrication method to obtain desired dimension and morphology is a great asset; and thus, modifying the

17

morphology for optimum photocatalytic efficiency is another major research for ZnO photocatalysis.

Regarding the morphology and photocatalytic activity of ZnO, there are various different opinions pointed out by different research groups. According to Tsang et al [57] the (100)/(002) intensity ratio is a key parameter in investigating photocatalytic activity. They emphasize that, at small (100)/(002) ratios a rather rod-like formation is observed among the crystal structure; on the other hand, higher (100)/(002) ratio indicates more of a plate-like morphology. He indicates that at high the (100)/(002) ratio better degradation rate of methylene blue is observed. The reason is associated with the influence of terminal polar faces which are claimed to be more active than the nonpolar surfaces [57]. They also claim that there is no distinct dependence of photocatalytic activity on particle size.

In a different study revealed by Chen et al [58] nanorod and nanoflower type structures are synthesized with a low temperature approach mixing zinc sulfate and sodium hydroxide in a solution where hydrazine is used reductant. The study shows that by changing the NaOH concentration, the morphology can be changed from rod like to flower like structures where the flower like structure shows a superiority in the degradation of 4-chlorophenol under UV irradiation. The reason of this high activity is associated with the high oxygen vacancy presence in the flower morphology, which acts as active center.

Another study that investigates the morphology effect on photocatalytic activity of ZnO structures is released by Simchi et al [61]. They synthesized ZnO structures with rod-like, flower-like and micro-sphere morphologies by employing facile hydrothermal method. The authors employed decolorization of Cl Acid Red 27 solution under sunlight to see the effect of different morphologies on the photocatalytic activity. The results indicate that rod like structure has superiority against the other two morphologies which in fact contradicts with the results published by Chen et al [58].

Yet in another study, Sin et al [62] performs fabrication of various ZnO morphologies using a surfactant free reflux method in which different morphologies are obtained only by adjusting the pH of the solution. As a result, spherical like, hexagonal like and pompon like morphologies are obtained. Degradation of pre-treated palm oil mill effluent (POME) under UV irradiation is used to compare the photoactivity of the given surfaces and the results show that pompon like morphology synthesized at pH 12 favors the highest activity among all morphologies [62].

There is a strong influence by some parameters in the growth of ZnO such as the type of precursor and it's concentration, temperature of the synthesis, addition of mineralizers, templates, pH of the solution, chelation agents, synthesis ratio and many others [19]. Through this, it can be understood that ZnO can be very rich in terms of its diversity in morphology.

Generally, the morphologies of ZnO are classified in terms of its dimension, such as 0 dimensional (0-D), 1 dimensional (1-D), 2 dimensional (2-D), 3 dimensional (3-D) structures [60]. For the 0-D structure, ZnO quantum dots can be given as example. The majority of the available structures are considered as 1-D, which include nanorods, needles, tubes, ribbons, helixes, wires, combs. Examples for 2-D ZnO structures are mainly nanoplate and nanopellet morphologies. For the 3-D structures it is possible to obtain flower type, dandelion type, snowflakes type ZnO morphologies [24].

Each type of classification is preferable to the other for several applications. ZnO morphology with 1D nanowire and nanotube structures show better results in mechanical endurance tests than other structures, making it a better candidate for actuators and nanoscale sensors [63]. Similarly, in another study published by Choy et al. [64] 2D nanosheet structure is a good candidate for photocatalytic applications. This remark is associated with the high surface area and polar faces of the 2D structures in which more contaminants can be adsorbed and reacted with the hydroxyl radicals. Yet in another study [65], it is noted that number of defects play important

role in trapping electron/hole pairs and promoting charge separation. With regard to this, 1-D nanowire structure with relatively low crystallinity and higher aspect ratio tend to have higher number of surface defects and oxygen vacancies and thus better photocatalytic performance [65].

2.3. ZnO Synthesis Methods

There are numerous methods available in the literature for the synthesis of ZnO structures with various morphologies. Mainly, the methods are subdivided in to two parts, which are solution based, and vapor based synthesis methods.

The solution based method offers a relatively easier and least energy consuming approach compared to vapor based synthesis. It also provides a better control over the size of the nanostructures [60]. Regarding to the solution based methods, the main idea of changing and controlling the morphology is based on altering synthesis variables such as reaction conditions, type of solvent and starting precursor material [66]. There are several methods for ZnO synthesis obeying to the solution based approach including sol-gel synthesis, solvothermal method, electrochemical deposition method, wet chemical synthesis, electrospinning, precipitation and several others [60].

Sol-gel technique is a very common method for the synthesis of metal oxide materials. It is one of the most attractive approach among the solution based methods for ZnO synthesis as it's a rather facile method to control morphology offering low cost and good repeatability at the same time [67]. Similarly, solvothermal method is another strong way to have control over the morphology, where an autoclave is employed as reactor vessel [68]. The precursor material is dissolved in solvent preferably with the presence of other chemical additives at relatively high temperature. By controlling the

temperature, reaction time and concentration of solvent material, different morphologies are possible to obtain with the solvothermal technique [69].

Another popular route among ZnO synthesis methods is the wet chemical method. In this route, a selected alkali hydroxide (preferably NaOH or KOH) is added to the zinc precursor solution preferably $ZnCl_2$ or $Zn(CH_3COO)_2$ with a given stoichiometric ratio in aqueous media. The addition of alkali hydroxide will yield $Zn(OH)_2$ formation in the form of white precipitates. Under moderate temperature $Zn(OH)_2$ will release water molecule to finally form ZnO [70]. If excess amount of alkali hydroxide is present in the media, formation of $Zn(OH)_4^{2-}$ complex is preferred instead of $Zn(OH)_2$. In this case, similar to the previous mechanism, $Zn(OH)_4^{2-}$ complex performs dehydration at high temperature, yielding ZnO crystallization in a rather different morphology than the previous case where lower alkali hydroxide concentration is used. Thus, in this method the morphology is strongly dependent on alkali hydroxide concentration, as at higher concentration of OH^- ions, complexation is favored among zinc atoms and upon dehydration different morphologies are observed [71]. The reaction mechanism for the wet chemical synthesis proposed by Satpati et al [70] is shown below.

$$Zn^{2+} + 2OH^- \rightarrow Zn(OH)_2 \qquad (2.13)$$

$$Zn(OH)_2 \rightarrow ZnO + H_2O \qquad (2.14)$$

$$Zn(OH)_2 + 2OH^- \leftrightarrow Zn(OH)_4^{2-} \qquad (2.15)$$

$$Zn(OH)_4^{2-} \rightarrow ZnO + H_2O + 2OH^- \qquad (2.16)$$
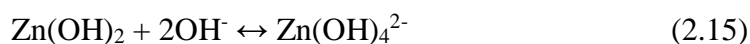
Using vapor phase routes to synthesize ZnO structures with various morphologies are also studied in the literature. These methods include physical vapor deposition (PVD), chemical vapor deposition (CVD), metal organic chemical vapor deposition (MOCVD), plasma enhanced chemical vapor deposition (PECVD), thermal

evaporation and several others [60]. These methods require a rather more complex set-ups than the solution based methods making them rather more expensive. Generally, the process of ZnO synthesis takes place upon a silicon substrate. Vapor phase Zn is released upon Si substrate in various environments to yield ZnO crystals. In some methods a metal catalyst is used to control the morphology [60]. Some of the ZnO fabrication methods in the literature with their starting materials and their resulting morphology are given in Table 3.

Table 3: Different ZnO Synthesis Methods from the Literature and their Corresponding Morphology [60]

Synthesis Method	Synthesis Material	Particle Size (nm)	Resulting Morphology	Ref..
Sol-gel	Zinc acetate dihydrate, oxalic acid dihydrate, ammonia, hydrochloric acid and absolute ethanol	20-25	Spherical	[72]
Microemulsion	Ethyl benzene acid sodium salt (EBS), dodecyl benzene sulfonic acid sodium salt (DBS), zinc acetate dihydrate, xylene, hydrazine and ethanol	80-300 in diameter	Nanorod	[73]
Wet Chemical	Zinc chloride, sodium hydroxide	300-500	Nanodisc	[74]
CVD	Zinc acetate di-hydrate, ethanol	Average diameter (90±27) and (564±150) in lenght	Nanorod	[75]
Sonochemical	Zinc nitrate hexahydrate, potassium hydroxide and cetyltrimethylammonium bromide	200–400 nm wide and a few nanometre thick	Nanoflakes	[76]
Solvothermal	Zinc acetylacetonate monohydrate, Triethanolamine, absolute ethanol and 1-octanol	Rod like particles 100 nm in length Spheres with 20 nm in diameter	Nano Shape: using Ethanol with TEA Nanorod: using Ethanol only	[68]
Electrochemical	Zn electrode, oxalic acid dihydrate purified, potassium chloride, sodium hydroxide and nitric acid.	150–200 nm long cylinders Spheres with 50–100 nm diameter	Combination of spherical and cylindrical particles	[77]
Microwave Assisted Hydrothermal	Zinc nitrate-6-hydrate, zinc acetate dehydrate, hydrazine hydrate and ammonia	50-150	Needle-type or flower type depending on the power of microwave.	[78]

23

2.4. Photocatalytic NO Oxidation Reaction on ZnO Surface

Starting from 2013 there are only few studies in the literature focusing on NO photooxidation reaction on ZnO surface. Almost all of the studies agreed on the importance of morphology, particle size and specific surface area for the oxidation performance; as well as, the importance of oxygen vacancies. The research papers initially focus on synthesizing one or more particular morphology with an indicated method such as solvothermal synthesis, sol-gel method or wet chemical synthesis and then focus on understanding the surface science behind the good or bad photocatalytic NO oxidation performance upon different morphologies.

Surface morphologies such as, rose-like, nanobars, flake-like, nanorods, flower type, spheres are obtained by different groups and their photocatalytic performances were evaluated. Almost all of the research groups adapted the ISO 22197-1 standard to evaluate the photocatalytic activity or a very close set up that is described in the ISO standard. Nevertheless, it is important to be aware of that each research group adapted different experimental conditions differing in their inlet NO concentration, irradiation type, relative humidity, reactor volume, reactor residence time distribution. Therefore, it is not a feasible approach to compare NO oxidation performance of different morphologies from different groups, but it is still a strong tool to have some idea about the morphology and NO oxidation performance relationship.

The first study on photocatalytic NO oxidation on ZnO photocatalyst is released by Wei et al [79]. In his research paper, a group of hierarchically structured ZnO hollow spheres is synthesized with solvothermal process using both template free and carbon template schemes[79]. The resulting ZnO samples have high surface area, providing better NO oxidation performance than commercial TiO_2 under UV and visible light irradiation experiments. The group claims that the microspheres have high photon absorption and good light scattering properties, which eventually increase the light

conversion efficiency. Thus, this high surface area hollow morphology favors the NO oxidation reaction [79].

Another research was carried out by Huang et al [80]. In this research, several morphologies including spindle-like, sunflower-like, dandelion-like, disk-like ZnO structures are obtained in a mixed solution of zinc nitrate and hexamethylenetetramine. Morphology control is sustained by manipulating the reaction time and changing the amount of 2-aminoethanol which is added as accelerant in the reaction mixture[80]. According to the research, sunflower morphology shows the highest photocatalytic activity in the NO oxidation reaction surpassing the commercial TiO_2 performance under UV irradiation. The reason of this high conversion with the sunflower morphology is associated with the high oxygen vacancy formation with the sunflower structure [80].

In 2014, Kowsari and Bazri [81] reveals a research fabricating 3D hierarchical rose-like structures using hydrothermal method with the presence of chiral ionic liquid (CIL) which is used to control the morphology. They test the rose like ZnO structures with their photocatalytic removal of NOx, SO_2 and CO pollutant gases under UV irradiation and observed that the highest NO oxidation conversion is achieved only by 23% with the rose-like structure. The templating agent CIL is being involved in the reaction mechanism and provides hydroxyl radicals to the system, which acts as oxidizing agent.

Yet in another research, Kowsari et al. [82] performs a similar study fabricating high surface area mesoporous hexagonal ZnO plates with different dimensions using a hydrothermal autoclave. However, this time, they use a functional ionic liquid (FIL) instead of chiral ionic liquid as templating agent to control the morphology. According to the group, due to the high surface area, better adsorption of pollutant gas is possible resulting in better conversion. The best structure among the synthesized samples shows 84% of NO conversion, which is much higher than the previous study released by Kowsari [82]. They point out the importance of reusability of the catalyst over time

and state that the accumulation of reaction intermediate products is the major reason of the catalyst deactivation in the gas phase. On the other hand, according to them, water is able to remove the surface intermediates; thus, catalyst in the aqueous phase suffers less from the deactivation problem.

In a series of papers, de la Cruz group examined various aspects of ZnO as a photocatalyst. In his first paper [83], he uses 4 different routes to synthesize different ZnO morphologies which are precipitation, solvothermal assisted PEG and sol-gel methods. The resulted morphology of the synthesis was bars with different sizes. The morphology synthesized by the sol-gel method gave the higher surface area, higher UV absorbance with lower particle size. Among the samples derived with the sol-gel route, one particular sample resulted in the highest photocatalytic activity in the NO oxidation reaction with %70 conversion. After that several other experiments conducted to observe the effect of humidity and the mass of the catalyst using the sample synthesized with sol-gel method. Once the mass of the ZnO catalyst coated on the surface is doubled, the resulting NO conversion increases up to 95%. In addition to that, another experiment is conducted with 70% relative humidity instead of 50% relative humidity [83]. The results show that for the first 90 minutes of the experiment, there is a slight increase in the NO conversion, but after some more time the conversion decreases down to 60%. This issue is associated with the competitive adsorption of H_2O and NO on the surface adsorption sites. These results were interpreted as the excess water vapor adsorbs on NO adsorption sites, which decreases the conversion over time.

In a subsequent publication the same group reported, 9 different ZnO samples are prepared by sol-gel method, where different morphologies were obtained by modifying the ZnAc and NH_4OH concentration [42]. The authors claimed that the size of the ZnO particle is highly depended on the ZnAc concentration in the synthesis. Samples with low ZnAc concentration have a lower growth rate and as a result of that, relatively lower particle size is obtained for the ZnO structures. In the end, samples with high ZnAc concentration resulted in finely distributed bar morphologies and

samples that contain lower ZnAc concentration during their synthesis resulted in agglomerates of semi-sphericals and flake-like particles. Eventually, higher NO conversion was reported with the small size bars, facilitating easy and convenient charge transfer[42]. The effect of humidity is once more clarified in detail in this research. They suggest that initially the ZnO surface is hydrophobic, but upon illumination and initiation of the photoreaction, the surface becomes hydrophilic in time, eventually a competition between the adsorption of NO and water molecules takes place.

Yet in another research, reported by the same group synthesized different morphologies were synthesized with hydrothermal process at relatively high temperatures [84]. Different morphologies obtained by changing the reaction time and the EDTA concentration, which is used as chelating agent in this synthesis. In total, 8 different ZnO samples are prepared by the authors, which include rods, flower-type and nanoplate morphologies. Among the samples, 6 of them resulted in nanoplate morphology, but their NO oxidation performance range from 43% to 95%. The authors observed that the ZnO sample with higher EDTA concentration and higher reaction time showed higher photocatalytic activity. The reason of this result remains unclear for the authors, but according to them the longer time for the hydrothermal treatment results in better formation of the particles with distinct shapes, which might possibly improve the activity. Moreover, according to the author, the small thickness of the nanoplates might promote the charge separation of the electrons and decrease the rate of recombination, thus increase the photocatalytic activity of the ZnO surface.

The last study that will be reviewed here about the NO photo oxidation reaction on ZnO surface is published by Chen et al [85]. In this study, mesoporous multishelled ZnO microspheres with hierarchically porous structures are synthesized using hydrothermal synthesis method and post calcination treatments. The resulting samples have high surface area and high crystallinity. In the study, the sample with highest photocatalytic activity yielded 77.3% of NO conversion. The authors associate the high NO oxidation conversion with the high crystallinity of the sample compared to

27

the others. According to them, at higher crystallinity samples, the photogenerated charges increase on the surface. Moreover, at high surface area higher frequency of multiple light reflection is possible in the surface resulting in higher light utilization efficiencies.

Table 4: Different ZnO structures studied in the literature with their NO Oxidation Performance

Synthesis	Reagents	Morphology	BET area (m^2/g)	% NO Conversion	Ref
Precipitation method with structural agents and accelerant	$Zn(NO_3)_2 \cdot 6H_2O$ $(CH_2)_6N_4$ C_2H_7NO	Spindle, Sunflower, Dandelion and Disk	39	55	[80]
Hydrated salt-assisted solvothermal method	$Zn(NO_3)_2 \cdot 6H_2O$ $(CH_2)_6N_4$ $Na_3C_6H_5O_7$	Spheres	607	70	[79]
Hydrothermal method using chiral ionic liquid	$Zn(O_2CCH_3)_2$ NaOH [TBA]$_2$[L-Tar]	Rose-like	33	20	[81]
Precipitation/ Hydrothermal/ Solvothermal assisted with PEG/ Sol-gel method	$Zn(NO_3)_2 \cdot 6H_2O$ $Zn(O_2CCH_3)_2$ NH_4OH	Agglomerates and Bars	16	70	[83]
Sol-gel method	$Zn(O_2CCH_3)_2 \cdot 2H_2O$ NH_4OH	Bars, Semispherical and Flake-Like	30	75	[42]
Hydrothermal route using functional ionic liquid	$Zn(O_2CCH_3)_2\{[CH_2CH_2]O_2 \ (mm)_2\}$	Hexagonal Mesoporous Plates	84	56	[82]
Hydrothermal method with EDTA as chelating agent	$Zn(O_2CCH_3)_2 \cdot 2H_2O$, KOH, EDTA	Nanoplates, Nanorods, Flowertype	6.5	95	[84]
Hydrothermal method using N-Acetyl-D-Proline as Template	$Zn(NO_3)_2 \cdot 6H_2O$ N-Acetyl-D-Proline	Micro Spheres	20	77	[85]

2.5. Photocatalytic NO Oxidation Reaction Mechanism on ZnO Surface

The photocatalytic NO oxidation reaction mechanism on ZnO surface is not yet known in detail unlike the reaction with the TiO_2 surface. According to Wei et al. [79] once the surface electron hole pair is generated with the energy of the light followed by the charge separation on the ZnO surface, the adsorbed water on the surface reacts with the photoinduced holes to generate hydroxyl radical ($OH\bullet^-$), while the adsorbed oxygen molecules capture the photogenerated electrons to form superoxide radical ($O_2\bullet^-$). The formed radicals have a key role in the NO oxidation on the ZnO surface acting as strong oxidants. According to the mechanism proposed by Wei et al, the hydroxyl radicals react with adsorbed NO molecules to form NO_2 and further reaction takes place with the radicals to form NO_3^-. The final product of the photocatalytic deNOx reaction is the adsorbed NO_3^- ion on catalyst surface, which diminishes the activity in time [79].

$$ZnO + hv \rightarrow (e^-_{CB}) + (h^+_{VB}) \qquad (2.17)$$

$$(h^+_{VB}) + H_2O \rightarrow OH\bullet + H^+ \qquad (2.18)$$

$$(e^-_{CB}) + O_2 \rightarrow O_2\bullet^- \qquad (2.19)$$

$$O_2\bullet^- + H^+ \rightarrow HOO\bullet \qquad (2.20)$$

$$NO + 2\ OH\bullet \rightarrow NO_2 + H_2O \qquad (2.21)$$

$$NO_2 + OH\bullet \rightarrow NO_3^- + H^+ \qquad (2.22)$$

$$NO_x + O_2\bullet^- \rightarrow NO_3^- \qquad (2.23)$$
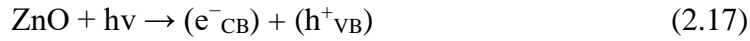
De la Cruz et al [84] propose another possible reaction mechanism for the NO oxidation on ZnO surface. In that study, they perform several scavenging experiments for photoinduced electrons, holes and the radical molecules to deduce the influence of those species in the NO oxidation reaction mechanism. During the experiments different scavenger molecules such as KI, $K_2Cr_2O_7$, isopropyl alcohol (IPA) and p-benzoquinone (BZQ) are added at certain times of the reaction. Those molecules acts as hole scavenger, electron scavenger, $OH\bullet^-$ scavenger and $O_2\bullet^-$ respectively. According to the results of the experiments, it is proposed that the photogenerated holes can react directly with adsorbed NO molecules on the ZnO surface, which is a distinct difference from the reaction mechanism with the TiO_2 surface. The resulting NO_2 can further react with adsorbed water to form NO_3^-. In addition to that, similar to the mechanism proposed by Wei et al [79], the superoxide radical ions can oxidize the adsorbed NO molecules directly to NO_3^-.

$$ZnO + hv \rightarrow (e^-_{CB}) + (h^+_{VB}) \qquad\qquad (2.24)$$

$$NO + 2\ (h^+_{VB}) + H_2O \rightarrow NO_2 + 2\ H^+ \qquad\qquad (2.25)$$

$$NO_2 + 2\ H^+ + H_2O \rightarrow NO_3^- + 2\ H^+ \qquad\qquad (2.26)$$

$$O_2 + (e^-_{CB}) \rightarrow O_2\bullet^- \qquad\qquad (2.27)$$

$$NO + O_2\bullet^- \rightarrow NO_3^- \qquad\qquad (2.28)$$
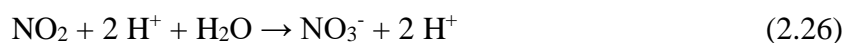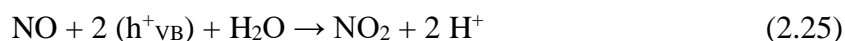
CHAPTER 3

MATERIALS AND METHODS

3.1. Materials

For the NO oxidation experiments a custom filled gas cylinder of 100 ppm NO stabilized in N_2 (purchased from Linde) was used as inlet gas. Ambient air was used to dilute the NO stream in the oxidation reaction. For the TiO_2 experiments commercial Degussa (Evonik) P25 was used.

3.2. ZnO Synthesis Method

All of the ZnO samples were donated from Admire Tech Company. The ZnO samples were synthesized with a proprietary method using wet chemical synthesis which is briefly described in Appendix B.

3.2.1. Sample Coating Methodology

The photocatalytic material in its powder form is placed in a bowl and mixed with deionized water until a uniform slurry is obtained. Unless otherwise indicated, 62.5 mg of photocatalytic material is used for 1 ml of deionized water to make the slurry. Once a homogeneous slurry is obtained, it is coated on a flat borosilicate glass test piece. To be able to distribute the slurry homogeneously on the glass with uniform thickness, the glass is circularly rotated just until the slurry dries. Once the slurry completely dries on the glass test piece, it is stored in oven at 75 °C to eliminate moisture.

3.3. Characterization Methods

3.3.1. XRD Characterization

The crystal structure identification of the synthesized ZnO samples were performed by the X-ray powder diffraction (XRD) technique in a Philips model PW 1840 X-ray diffractometer operated at 30 kV and 24 mA using Ni-filtered Cu Kα radiation source. The scattering angle is recorded from 5° to 90°. Also the particle size calculation with the Scherrer equation is conducted using the pattern obtained from the diffractometer.

3.3.2. BET Characterization

The specific surface area of the samples was determined in accordance with the BET method in a Micromeritics Tristar II surface area and porosity analyzer measuring the N_2 adsorption-desorption isotherms at -196°C. The samples were degassed at 120°C for 4 hours before the experiment using the Micromeritics VacPrep 061 Sample Degas System.

3.3.3. SEM Characterization

Scanning electron microscope (SEM) was used to characterize the morphologies of the obtained products. Majority of the analysis is performed with a QUANTA 400 F Field Emission SEM instrument with 1.2 nm resolution present at the ODTÜ Mer-Lab, while AT 03-04 and 05 samples are analyzed at ODTÜ Chemical Engineering Dept. Laboratories with TESCAN Vega 3 SEM instrument.

3.4. NO Oxidation Experimental Set-up

NO oxidation method is a standard test method to evaluate the air purification performance of the photocatalytic semiconductor materials. In order to obtain accurate and reliable results, an experimental set-up is necessary that fully complies with the descriptions given in ISO 22197-1:2007 (E) manual. The existing set-up consists of a photoreactor, a chemiluminescence NOx analyzer, mass flow controller units, a light source, compressed gas cylinder for the source of pollutant test gas and a compressor for the air supply [86], [87].

Since the concentration of the NO gas fed to the system is very low, the system has to be constructed with materials having low NO adsorption affinity. In addition to that, materials with high resistant to UV irradiation must be picked to avoid possible harms of UV to the system. Considering this, plexiglass is used for the fabrication of the photoreactor and the rest of the system consists of stainless steel equipment. Special attention was given to have a constant flow distribution in the reactor for each experiment. Thus, small barriers are placed at the entrance and the exit of the reactor and the possible channeling effects are avoided with an appropriate design. A quartz window is placed on top of the reactor to transmit the UV irradiance to the system. Inside the reactor, a small rectangular groove is present to hold the coated glass test piece. The distance between the test piece and the quartz glass is set as 5 mm as indicated in the ISO standard. The glass test piece have dimension of 50x100 mm which perfectly fits to the rectangular groove. Special attention is given for the glass test piece to perfectly fit to the empty spot to avoid possible channeling effect which will change the residence time distribution of the reactor.
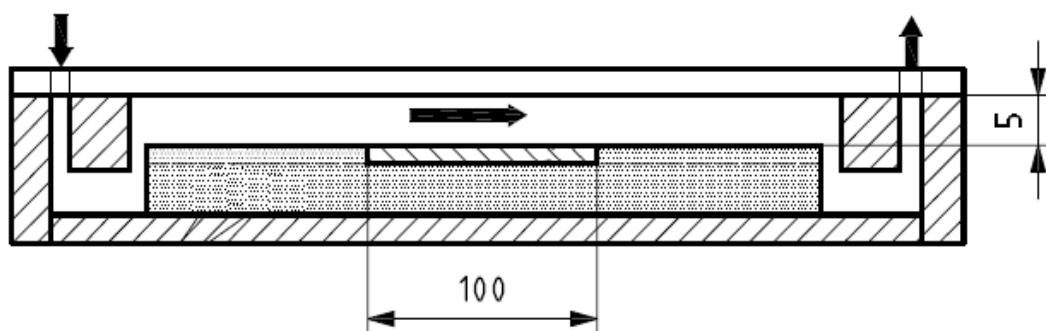
Figure 5: Crossectional View of the Plexiglass Photoreactor [27]

An UV-A lamp with wavelength of 365 nm was used as the light source. A chemiluminescence NOx analyzer as specified in the standard is used for measuring the NO concentration at the reactor outlet. For this purpose, Model 42i NO-NO_2-NOx Analyzer from Thermo Fischer Scientific is used.

The flowrate of the NO gas in the system and the air flowrate is controlled by mass flow controllers (Teledyne). To be able to supply some water vapour to the system, some part of the air stream is connected to a humidifier before it reaches to the reactor. To do that, the air stream is divided into two. Thus, in total 3 mass flow controller units are used, where 1 unit for the NO stream and 2 units for the air streams.
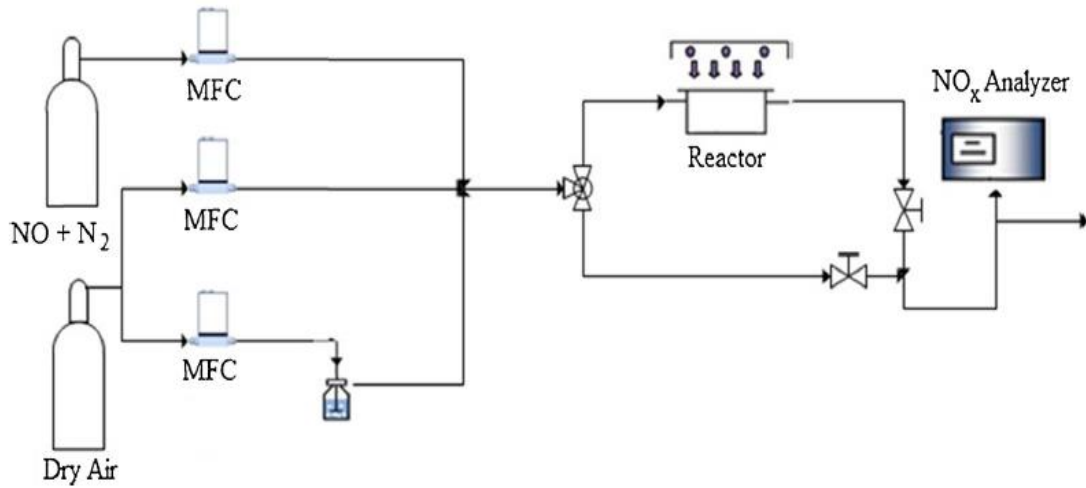
Figure 6: NO Oxidation Experimental Setup adapted from [87] with permission

3.4.1. NOx Analyzer Principle with the Chemiluminescence Method

The concentration of the NO coming out of the reactor is detected with the chemiluminescence method which is based on the principle that nitric oxide and ozone react to produce light with an intensity linearly proportional to the NO concentration. In the system, the intensity of the characteristic luminescence of the light is measured by a photomultiplier tube and the NO concentration is measured with the measured light intensity.

$$NO + O_3 \rightarrow NO_2 + O_2 + h\nu$$

The NOx analyzer can proceed with two available modes. The first mode is the manual NO mode where only the NO concentration is monitored. This mode is very useful for data acquisition at short time range as it is possible to obtain NO concentration at every second. The incoming gas stream by-passes the NO_2 to NO converter and just measures the NO content through the reaction with ozone. The second mode of the instrument is the Auto NOx mode which allows to obtain data for both NO and NO_2 concentrations. However, the NO_2 must be converted into NO before it can be measured with the chemiluminescent reaction. Thus, the gas stream passes through

NO₂ to NO converter at every 10 seconds so that all the NO_2 in the system is converted to NO in the converter at about 325 °C with Molybdenum catalyst and the resulted NO content is sent to the reaction chamber to react with ozone. This time the sum of NO and NO_2 is measured which is denoted as NOx concentration. The NO_2 concentration is calculated simply by substracting the measured NO concentration from the NOx concentration. This cycle is controlled by a selonoid valve at this mode and this cycle repeats itself at minimum 10 seconds.

The required ozone for the chemiluminescent reaction is generated at the ozonator. The ozone then reacts with the NO in the reaction chamber to yield excited NO_2 molecules. Finally, the generated luminescence is detected with the help of a PMT tube.
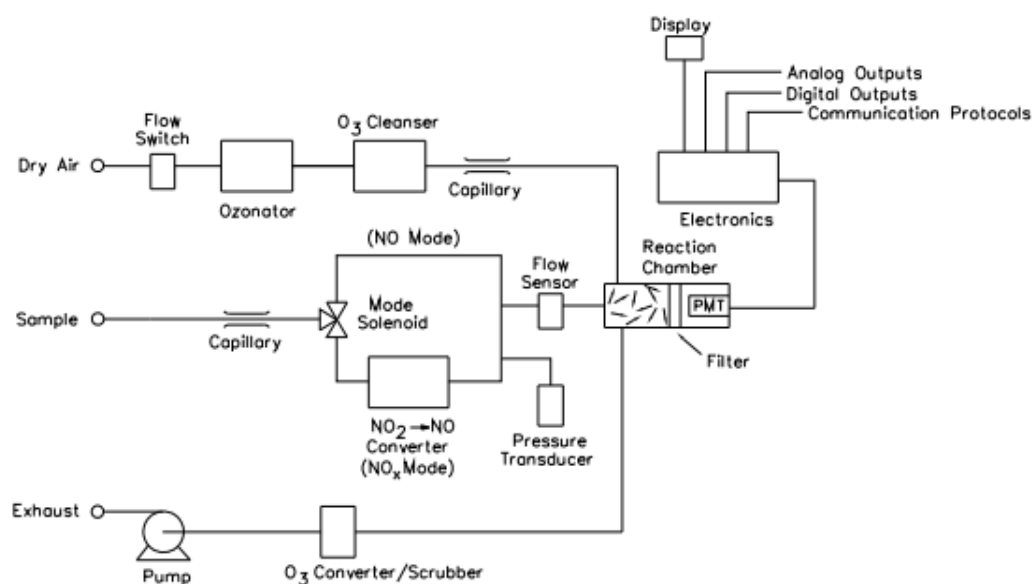
Figure 7: NOx Analyzer Operation Flow Scheme [88]

3.4.2. NOx Oxidation Experimental Procedure

According to the ISO standard, the coated test piece must be treated in the beginning to remove the organic matter on the catalyst surface. For this purpose, the test piece is first irradiated with the UV lamp for enough time to decompose the residual organic matter at the catalyst surface. The treated catalyst test piece then placed on the reactor to start the experiment. Before conducting the experiment, the test gas first directly goes to the NOx analyzer through by-passing the reactor. By doing this, the inlet concentration of the NO test gas is determined and the system reaches to steady state before the experiment. A certain amount of humidity is given to the system by adjusting the humid air and dry air flowrates using the air MFC units.

A simple calibration is performed before running the experiment. The desired value of the NO concentration is first adjusted using the MFC units. During the calibration, the inlet stream by-passes the reactor using a valve and directly goes to the NOx analyzer. The system reaches steady state in the order of a minute. Then, the expected NO concentration, which is set by the MFC units is checked with the NOx analyzer displaying monitor. The experiment is ready to run if the difference between the calculated and displayed NO concentration is in an acceptable order which is in the order of 50 ppb.

Once the flow is changed from by-pass to the reactor stream, a very quick dilution of the NO gas takes place in the empty reactor volume. The dilution of the NO concentration recovers itself within seconds depending on the flowrate of the inlet stream. Using the signal coming from this fast dilution, the residence time distribution data of the reactor is acquired. In the ISO 22197-1 standard description the negative peak coming from the fast dilution is mainly associated with the adsorption of the NO molecules. However, this negative peak gives information about the time that NO molecules spend in the photoreactor. Thus, the residence time distribution data

acquisition is independent from the ISO standard. The experiment can now proceed with the NO oxidation reaction procedure from now on.
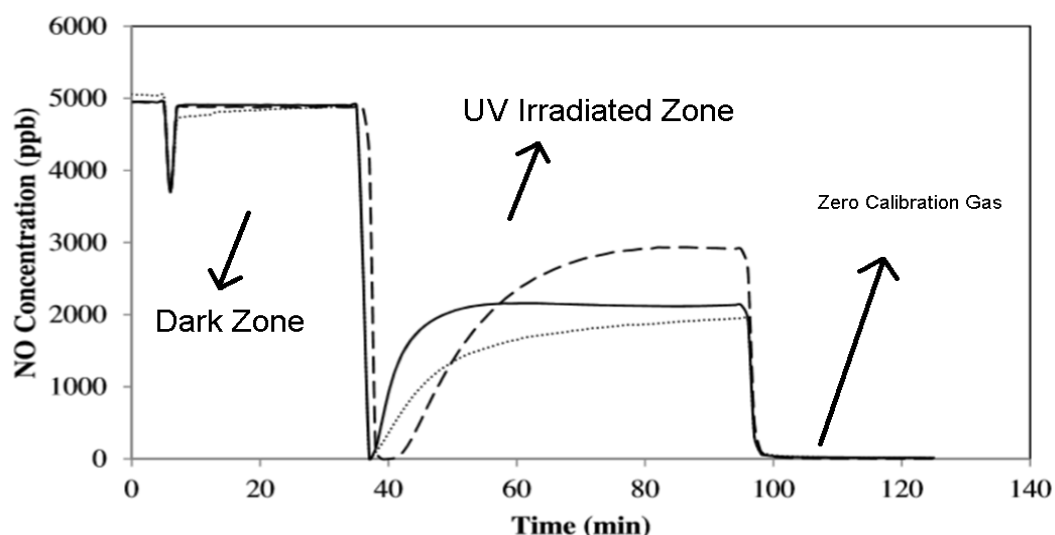
Figure 8: An illustration of a possible NO Oxidation reaction resulting data [87]

The NO oxidation experiment is investigated in three stages. In the first stage the test gas which is composed of NO gas diluted at humid air is allowed to flow into the photoreactor with a known concentration under dark conditions. The top side of the reactor is covered with aluminum sheet to avoid penetration of light. At this stage the adsorption of NO molecules to the catalyst surface takes place. This stage is maintained for 30 mins until the system reaches steady state. In the second stage, the aluminum foil is taken out and the UV irradiation is given from the top of the reactor where the lamp directly sees the quartz window. The light intensity and the distance between the light source and the reactor is fixed for all experiments. Once the UV irradiation starts, a sharp decrease in the NO content is observed. The reason of this sharp decrease can be associated with the fast reaction of the already adsorbed NO molecules at the dark zone. The system reaches steady state in approximately 1 hour

38

and the NO concentration is recorded continuously. In the third and final stage the zero calibration gas is fed to the system which is dry air to clean the reactor system and the catalyst surface from the residual materials. A typical NO experiment result is demonstrated at Figure 8. The NO and NO_2 concentration is continuously recorded in a computer and an excel spreadsheet is prepared for further calculations.

CHAPTER 4

RESULTS & DISCUSSION

This section of the thesis is organized as follows. First, material characterization by XRD, SEM and BET analyses are reported. Then, the NO photooxidation activity data were presented and interpreted in the light of characterization data.

4.1. XRD Analysis

Using the diffraction peak positions and intensities the possible polymorphs were tried to be identified. It is noted that XRD patterns of each sample have the same peak positions, but the peak intensities as well as broadenings may vary from sample to sample showing the degree of crystallinity and the orientation of the indices. The XRD patterns of the 19 samples are having same peak positions showing compatibility to wurtzite structure according to the JCPDS database Card No. 36-1451 except for AT 16 which has a small peak at the early angles showing an impurity in the synthesis. Considering the present impurity, AT 16 is not used at the further experiments. Apart from that, it might be concluded that wurtzite is the only polymorph that is seen in the samples.
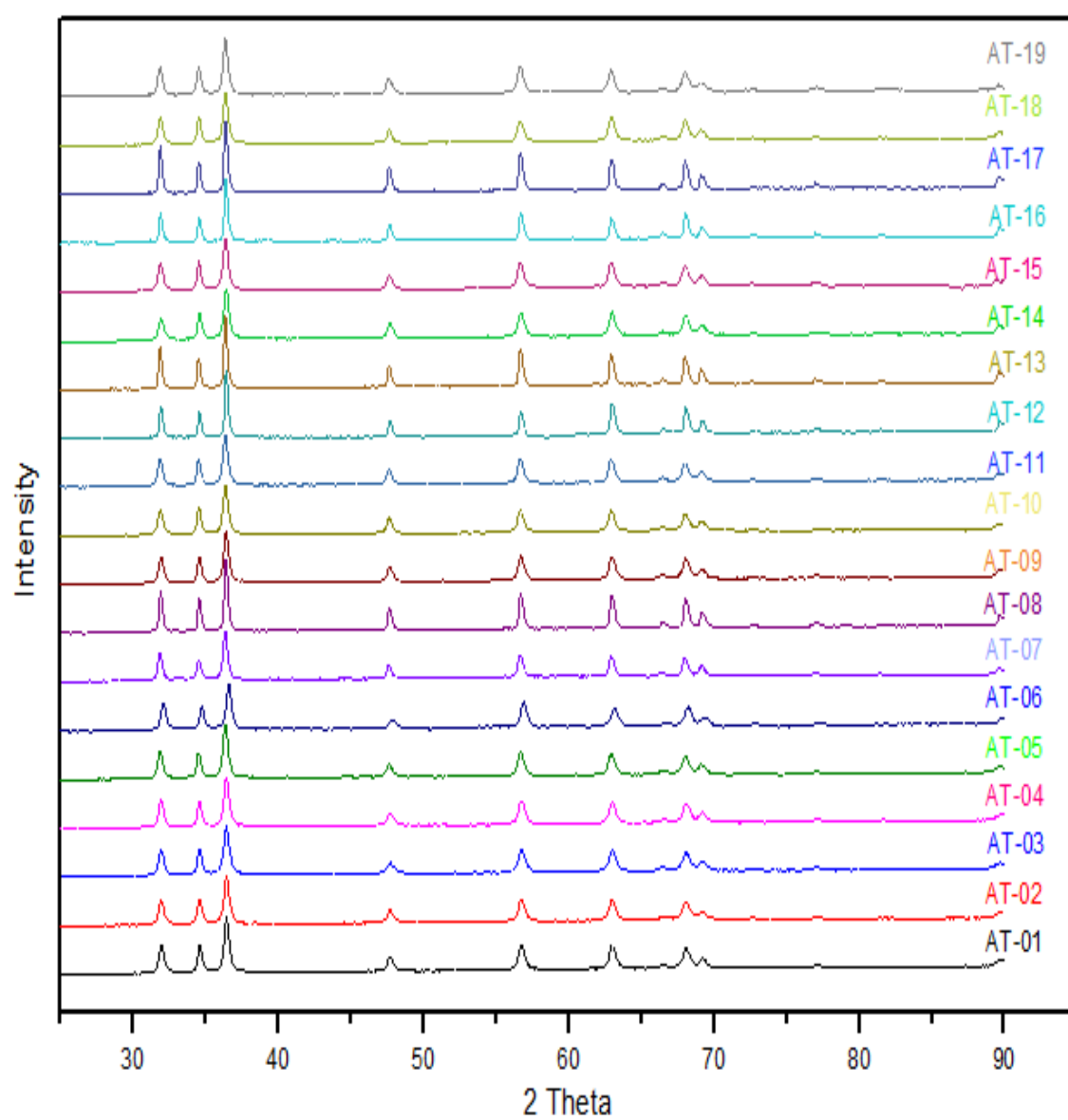
Figure 9: XRD Patterns of the ZnO Samples
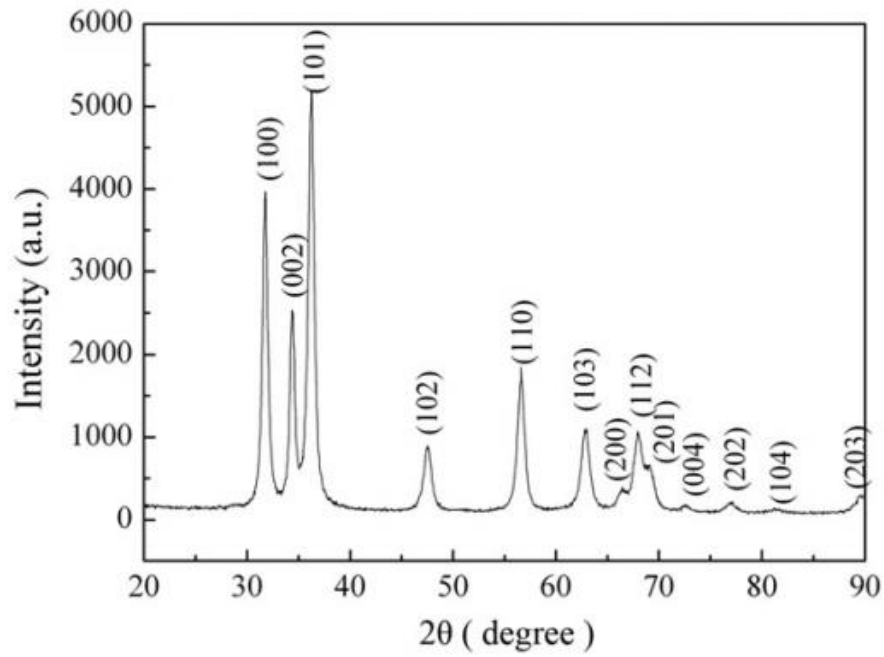
Figure 10: JCPDS Card Number 79-2205 Hexagonal Wurtzite XRD Pattern adapted from [89] with permission
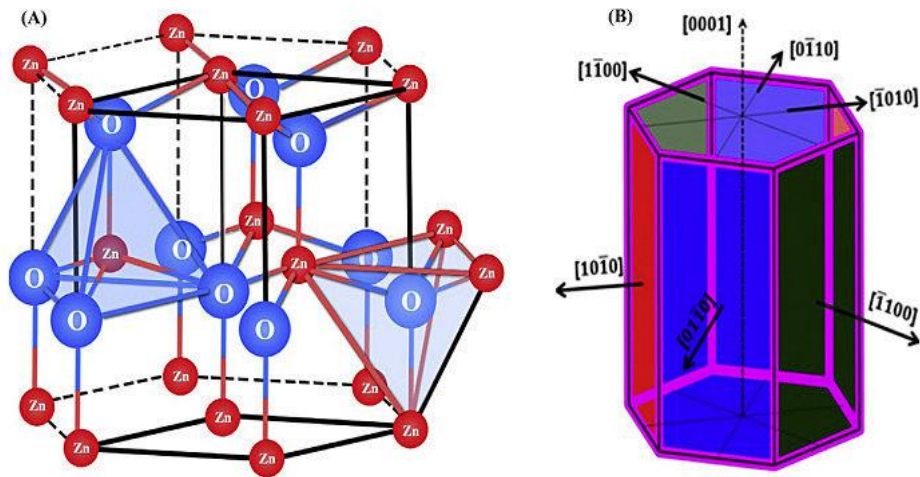
Figure 11: Hexagonal Wurtzite Crystal Structure of ZnO and its Crystallographic Faces adapted from [90] with permission

4.1.1. XRD Analysis

The XRD patterns are available for each ZnO sample as given at Figure 10. Considering their plane intensities, it is seen that the (101) plane had the highest intensity among the peaks. Nevertheless, the relative intensity of other planes are varying for different samples. An analysis is conducted by calculating the intensity ratio of each plane with respect to intensity of the (101) plane to have an idea about the direction of the crystal growth through the XRD relative intensities. This analysis reveals the dominant crystal orientation for each ZnO crystal structure. This information can be used in the NO oxidation reaction and find out the most favored crystal orientation in the ZnO samples by comparing their rate of reaction. This analysis is performed individually for each sample as independent from their synthesis stoichiometry. The SEM images are later used to validate the results coming from this analysis.

Generally, higher plane intensities indicate larger number of planes in that specific direction. For instance, relatively higher intensity at the (100) plane is expected to favor rather hexagonal rod like structure, which in fact resembles the wurtzite structure itself. In other words, a distinct growth in the z-axis is expected at higher (100) intensities. On the other hand, high intensity for the (002) plane indicate a growth in the x-axis, which is expected to be seen as a growth from the sides of the particle. With a similar analysis, it is also possible to see effect of relative intensity at the other planes such as (110), (103) and (112).
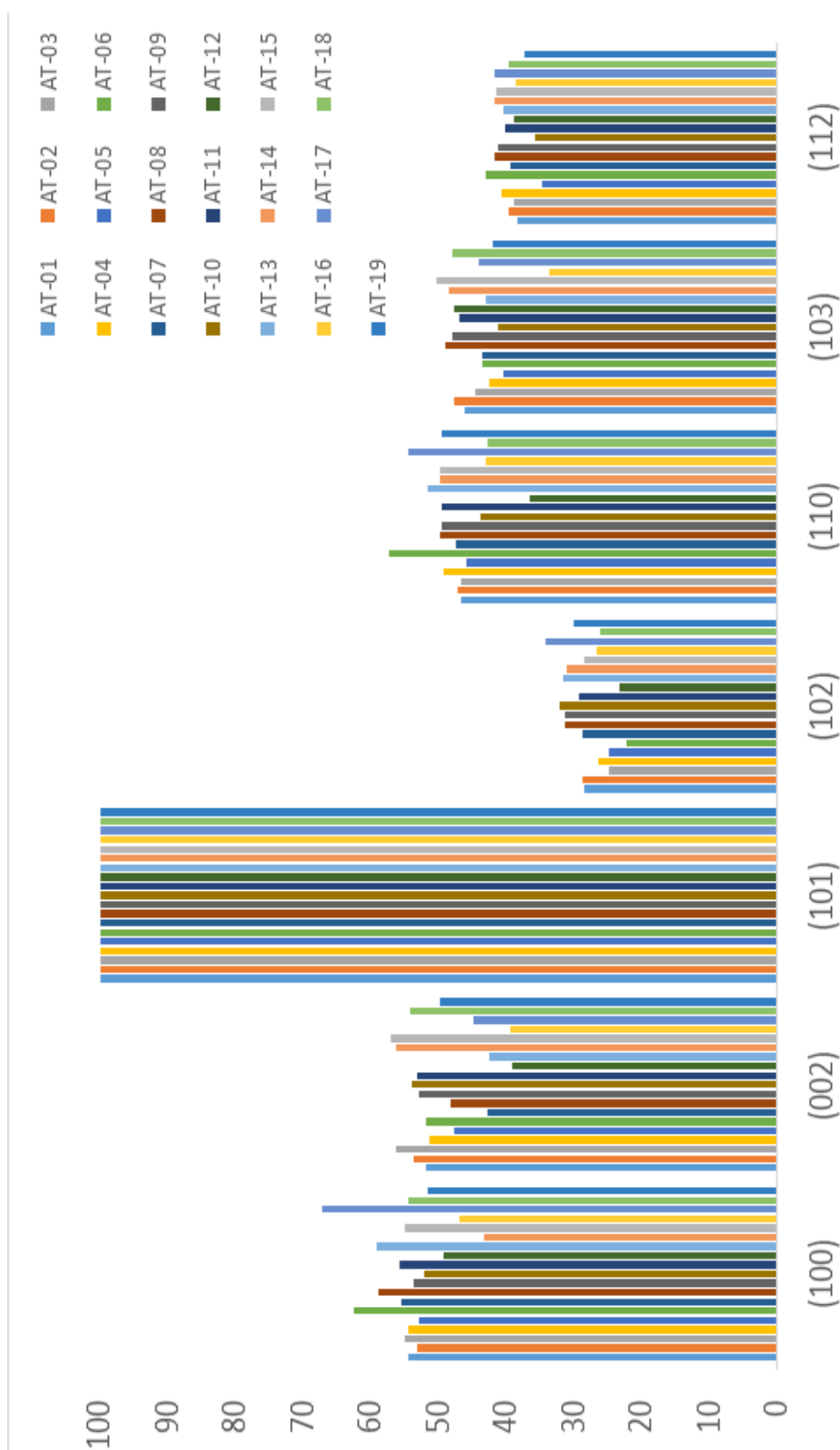
Figure 12: XRD Relative Intensity of the Planes with Respect to Maximum Intensity Calculation

It is clear that the (101) plane has the highest intensity for each sample with no exception, but there is a competition in relative intensities for several other planes mainly in between (100), (002), (110), (103) and (112). It is observed that for the samples synthesized at relatively more acidic media (i.e. at lower NaOH:ZnAc ratio), the presence of (002) plane intensity is rather low compared to the (100) plane. On the other hand, the relative intensity of (002) is as much as the (100) plane intensity at the samples synthesized at a more basic reaction media (i.e. at higher NaOH:ZnAc ratio). The calculated relative intensity of the planes with respect to the maximum plane intensity is demonstrated in Figure 13.

A simple ranking system is used to classify the ZnO samples with respect to their XRD relative intensity data. In short, samples following a distinct order of ranking are expected to have similar morphology. For each sample, the first 5 highest peaks after the (101) plane are chosen considering their relative to maximum intensity values as it is shown in Table 5.

To have a better classification, it is also important to consider the limited precision of the XRD instrument; thus, a sensitivity value is determined using the intensity coming from the noise observed at the XRD pattern. After accounting for this intensity of the noise, for some specific samples, two indices are considered as having the same relative intensity.

Several ZnO samples with certain NaOH:ZnAc stoichiometry are found to follow a particular order in their XRD relative intensities which are classified as Group 1 and Group 2. One of the main assumption during the classification is that; if one of the plane is one rank higher or smaller than the groups order, it is still considered as acceptable to be classified at the same group. This assumption made it possible to decrease the total number of groups down to 2.

Table 5: Classification of the ZnO Samples With Respect to Their XRD Relative Intensity Analysis

NaOH:ZnAc Stoichiometry	Sample	1	2	3	4	5	Group #
1:1	AT 07	(100)	(110)	(103)	(002)	(112)	1
	AT 12	(100)	(103)	(002)	(112)	(110)	1
1.5:1	AT 08	(100)	(110)	(103) (002)	(112)		1
	AT 13	(100)	(110)	(103) (002)	(112)		1
	AT 17	(100)	(110)	(002)	(103)	(112)	1
2:1	AT 06	(100)	(110)	(002)	(103)	(112)	1
	AT 01	(100)	(002)	(110) (103)	(112)		2
	AT 02	(100) (002)	(110) (103)	(112)			2
	AT 03	(002)	(100)	(110)	(103)	(112)	2
	AT 04	(100)	(002)	(110)	(103)	(112)	2
	AT 05	(100)	(002)	(110)	(103)	(112)	2
2.5:1	AT 09	(100) (002)	(110)	(103)	(112)		2
	AT 14	(002)	(110)	(103)	(100)	(112)	2
	AT 18	(100) (002)	(103)	(110)	(112)		2
2.76:1	AT 19	(100)	(002)	(110)	(103)	(112)	2
3.0:1	AT 10	(002)	(100)	(110)	(103)	(112)	2
	AT 15	(002)	(100)	(103) (110)	(112)		2
3.5:1	AT 11	(100)	(002)	110)	(103)	(112)	2

4.1.2. Particle Size Calculation with Scherrer Equation

Based on the XRD patterns of the ZnO samples, particle sizes were determined using Scherrer equation. Since the Scherrer equation is valid only under some certain non-practical assumptions, in this study, it is not used as a quantitative approach to determine the volume average particle size of the ZnO particles. But, it is used to qualitatively compare and have idea about the volume average particle size of the samples. The calculated volume average particle size of the samples are presented in Table 6.

4.2. SEM Analysis

SEM images were taken from each synthesized ZnO samples. The images are presented with respect to their corresponding group number. In short, relatively bigger and distinct particles are observed with hexagonal structures at the samples with the Group number 1. On the other hand, rather flake like structures with relatively smaller particle size are observed for the Group 2 samples. Although most of the samples have a particle size at the macro scale, the samples synthesized with NaOH:ZnAc ratio of 2:1 yields particles in the nanoscale as it can be observed at their SEM images.

The results coming from the XRD relative intensity analysis can be associated with the SEM images of the samples. For example, the Group 1 samples particularly have the (100) plane at the higher ranks which have favored a distinct growth on the z- axis, besides those particular samples have their (002) plane at relatively lower ranks. As a result of that distinct hexagonal particles are formed mainly for Group 1 samples. On the contrary, for the Group 2 samples, the (002) relative intensity has either first or second position in the ranking system. This property can be associated with the apparent domination of the flake-like structure at the Group 2 samples.
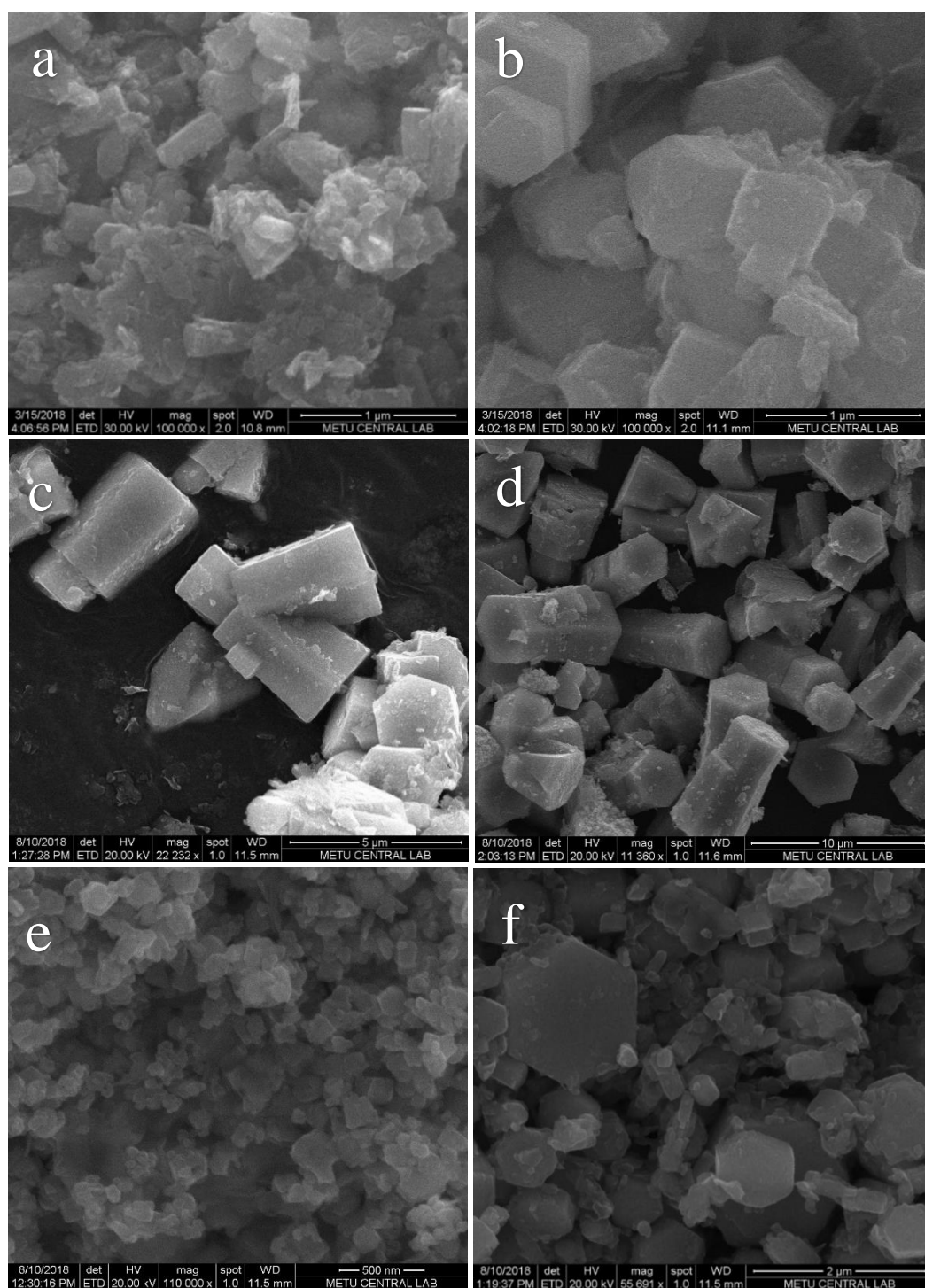
Figure 13: SEM images of Group 1 ZnO Samples a) AT 07, b) AT 08, c) AT 13, d) AT 17, e) AT 06, f) AT 12
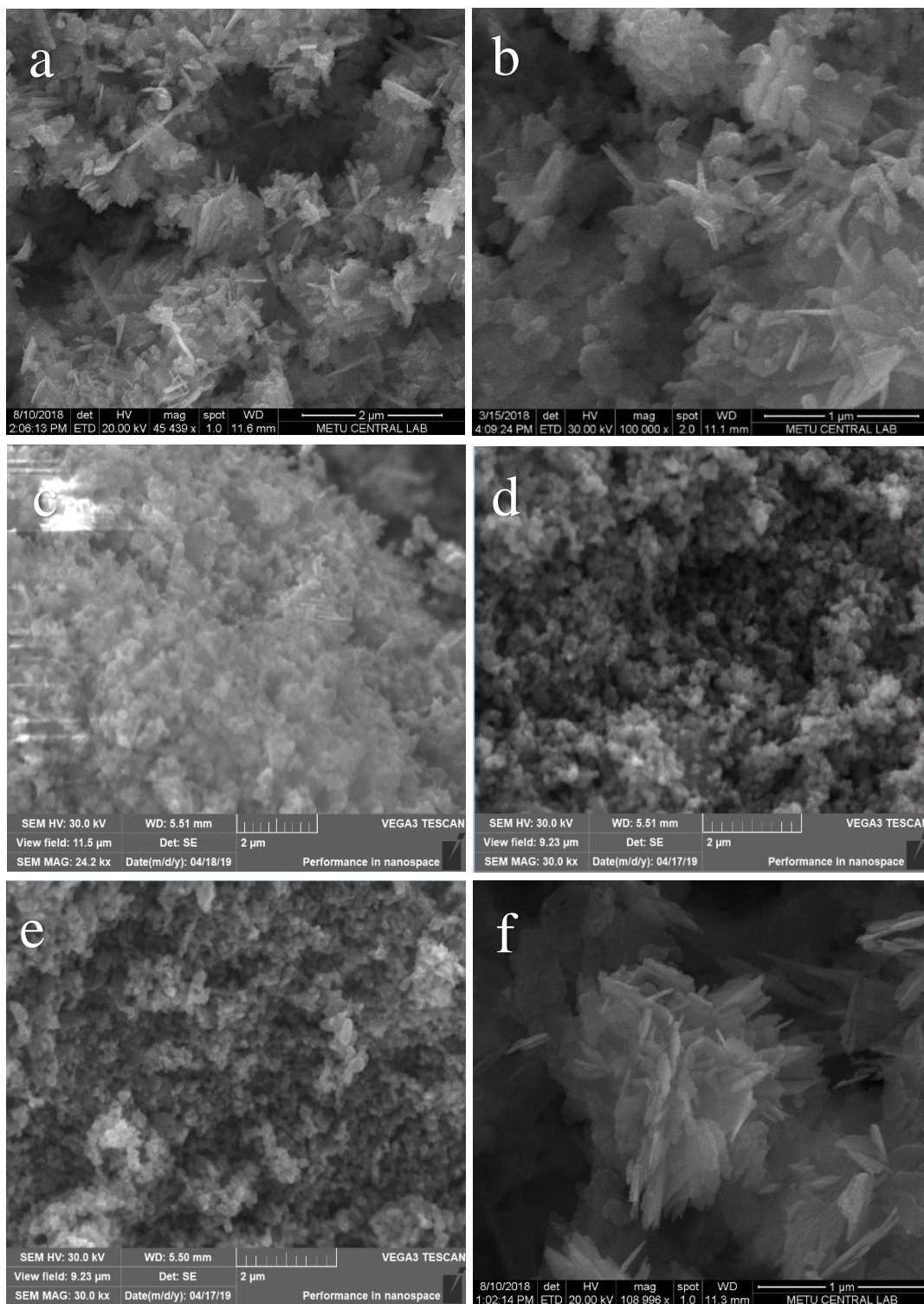
(* Figure 14 Continued)
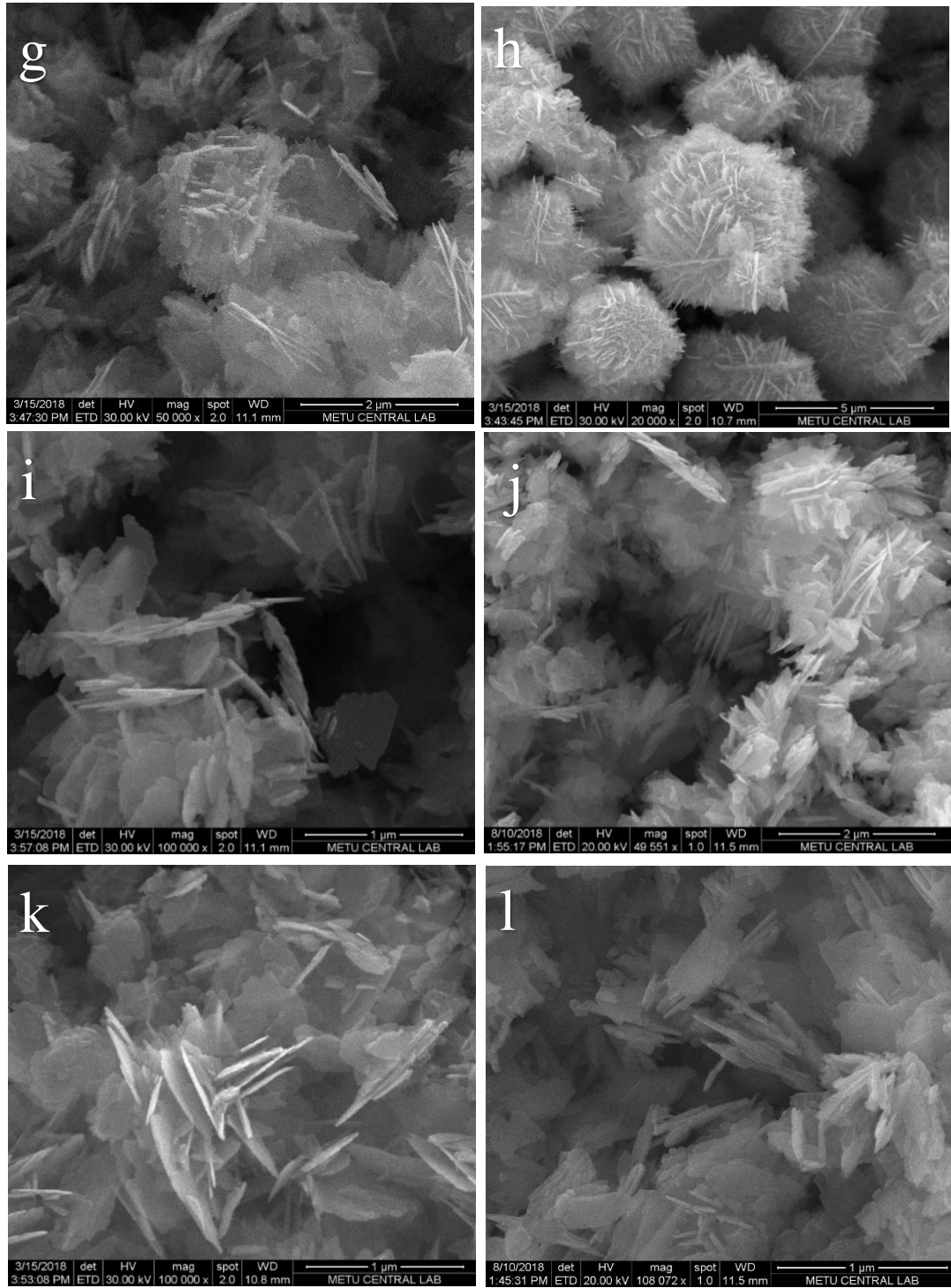
Figure 14: SEM images of Group 2 ZnO Samples a) AT 01, b) AT 02, c) AT 03, d) AT 04, e) AT 05, f) AT 09, g) AT 18, h) AT 19, i) AT 10, j) AT 15, k) AT 11, l) AT 14

51

4.3. BET Analysis

The BET surface area of the synthesized ZnO samples are presented in Table 6. Mainly, the surface area of the samples range from 1 m^2/g to up to 16 m^2/g. From the analysis it is found that except for AT 06, the samples from group 1 have considerably smaller BET area, indicating the high particle size. On the contrary, the samples with Group 2 yields relatively higher surface area. The results can be associated with the SEM images and XRD analysis. The exception of the AT 06 can be associated with its very small particle size compared to the other Group 1 samples. Using the BET area results, it is possible to calculate the surface average particle size of the samples using the bulk density of ZnO. The calculated surface average particle size of the samples are presented at Table 6.

Table 6: Morphology, BET Area and the Particle Size Analysis of Corresponding ZnO Samples

Group	Sample	Morphology	BET Area (m^2/g)	Surface Average (BET) Particle Size (nm)	Volume Average (XRD) Particle Size (nm)
1	AT 07	Hexagonal	5.73	1188.5	22.5
1	AT 12	Hexagonal	4.30	1583.8	29.9
1	AT 08	Hexagonal	1.22	5582.3	28.1
1	AT 13	Hexagonal	1.06	6424.9	30.3
1	AT 17	Hexagonal	3.65	1865.8	30.2
1	AT 06	Hexagonal	12.5	544.8	19.8
2	AT 02	Flake	11.1	613.5	17.9
2	AT 03	Flake	9.73	699.9	16.9
2	AT 04	Flake	10.0	681.0	19.0
2	AT 05	Flake	8.74	779.2	19.8
2	AT 01	Flake	8.26	824.5	19.5
2	AT 09	Flake	14.6	466.4	19.9
2	AT 14	Flake	15.2	448.1	19.6
2	AT 18	Flake	10.5	648.6	19.4
2	AT 19	Flake	11.7	852.1	20.2
2	AT 10	Flake	15.6	435.2	19.0
2	AT 15	Flake	14,9	457.1	19.2
2	AT 11	Flake	13.9	491.7	19.5

4.4. Photocatalytic NO Oxidation Experiments

4.4.1. Residence Time Distribution Experiments

The purpose of this system is to benchmark different catalysts with respect to their NO oxidation capabilities and to reveal the appropriate morphology for the NO oxidation reaction. However, it must be noted that, it is not possible to compare two experimental results with different RTD behavior. Hence, RTD analysis is necessary. Similar RTD behavior was obtained at particular inlet concentrations meaning that the amount of time that the gas molecules could spend inside the reactor are almost same with this newly constructed reactor. This feature is important for the repeatability of the experiments.

The experiments were conducted at 1L/min inlet gas flowrate with 1000 ppb, 2500 ppb and 5000 ppb inlet NO concentrations using a blank test piece which perfectly fits to the rectangular groove in the photoreactor. During the experiments, barriers with different thicknesses are placed to the inlet and outlet of the photoreactor to modify the residence time. The barriers are used to increase the residence time by providing more mixing to the system.
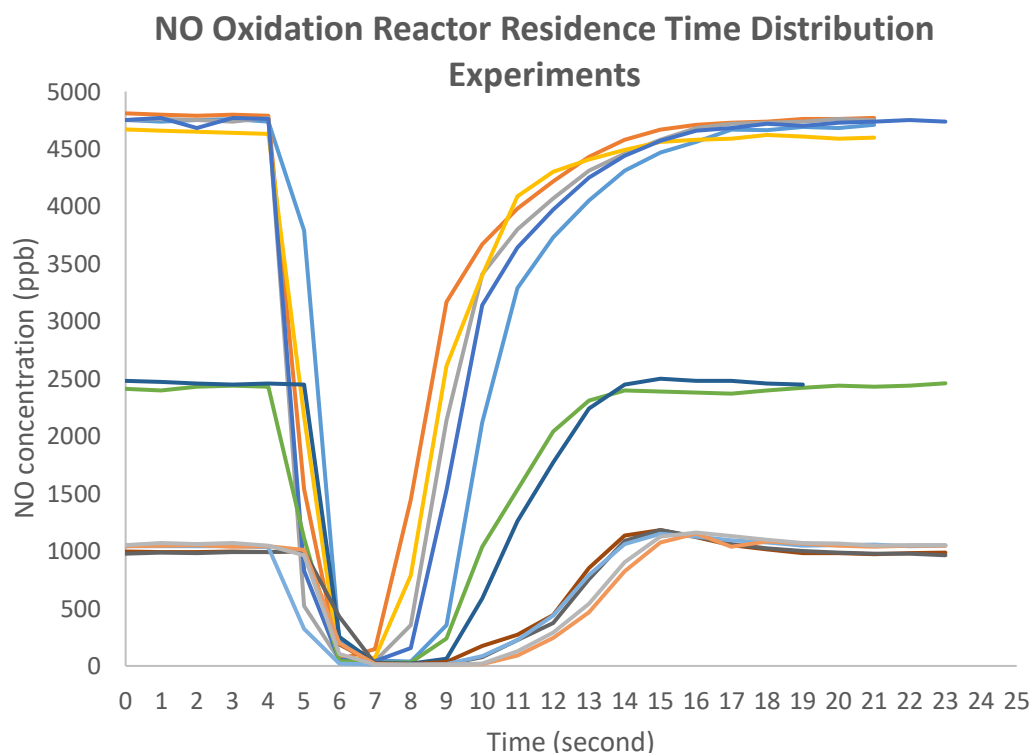
Figure 15: Residence time distribution experiments on the NO Oxidation reactor

The RTD experiment is conducted at the first stage of the NO oxidation experiment. Once the inlet flow stream is switched from by-pass to the reactor side, the inlet NO concentration is exposed to a sudden dilution due to the air present in the photoreactor. This sudden dilution is recorded using the NOx analyzer with a data acquisition in the order of second. It is seen that at the first 3-4 seconds of the dilution, very little amount of the NO content reaches to the NOx analyzer. Then, the NO concentration starts to recover itself gradually with the continuous flow and eventually reaches steady state in the following 7-8 seconds. Thus, it is observed that, once the NO concentration is diluted in the empty reactor, it takes around 10-12 seconds to fully recover its initial concentration and reach steady state. This result also tell us that, the time resolution of this system is in the order of 10-12 seconds. Hence, any experiment with shorter than this time resolution may not give the accurate results.

The $\Delta C_{NO}/\Delta t$ vs time curve is plotted to see the change of NO concentration just after the inlet gas enters the photoreactor and to calculate the mean residence time of the NO molecules in the photoreactor at different inlet NO concentrations. From Figure 16, it can be roughly said that at 5000 ppb inlet concentration, PFR behavior is seen at the first 4 seconds, while CSTR behavior becomes predominant for the rest of the process. On the other hand, for both 2500 ppb and 1000 ppb inlet NO concentrations, CSTR behavior is predominant from the beginning to the end of the experiment. Thus, CSTR assumption can be used for the reactions with relatively lower inlet NO concentrations. The calculated mean residence time for 5000 ppb, 2500 ppb and 1000 ppb inlet concentrations are 3.31, 3.71 and 5.59 seconds respectively.
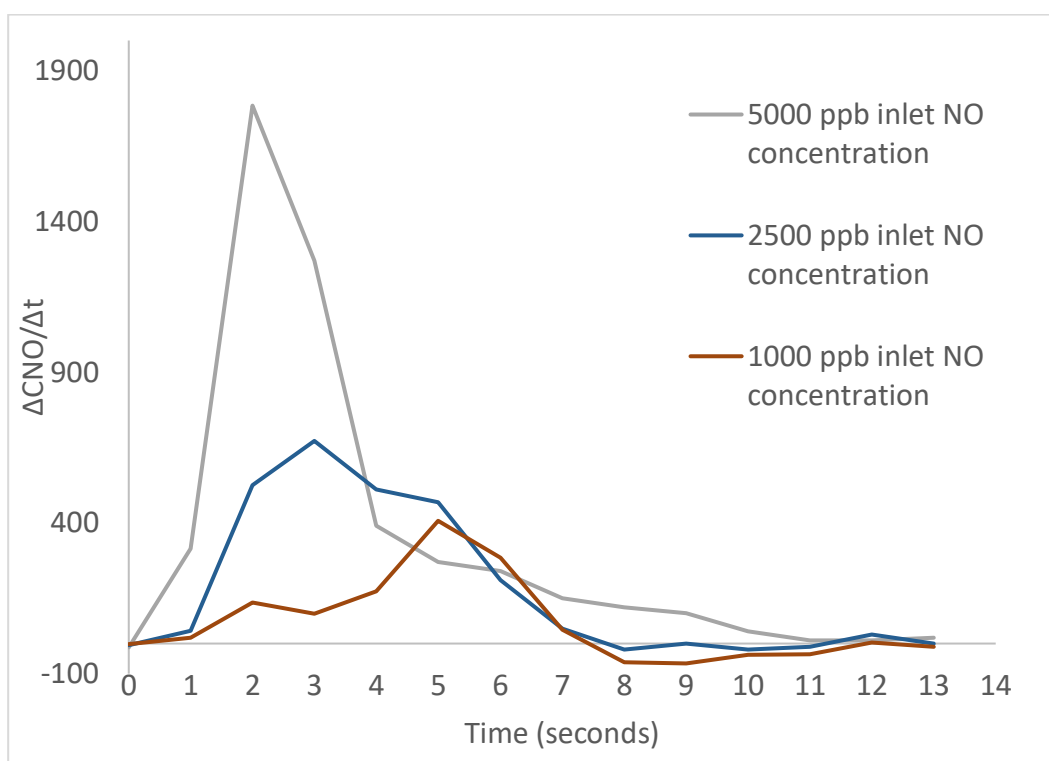
Figure 16: Rate of Change of NO Concentration with Time during the RTD Experiments at Different Concentrations

4.4.2. Evaluating Photocatalytic Activity using NO Oxidation Experiment

Each sample was exposed to standard photocatalytic NO oxidation experiment to measure its photocatalytic performance and the results are compared with the performance of commercial TiO_2. The rate of reaction is calculated on per gram catalyst basis using CSTR assumption. Inlet concentration of NO stream is selected as 500 ppb for all experiments. 50% humidity is supplied to the inlet stream for each experiment and 1L/min of inlet gas flowrate is used.

The results of the NO oxidation reaction are presented in the Table 7. The average NO oxidation rate for the samples at Group 1 is calculated as $2.86x10^{-3}$ (µmol/gcat.sec); while, the average NO oxidation rate for the Group 2 samples are calculated as $2.23x10^{-3}$(µmol/gcat.sec). From this analysis, it can roughly be said that hexagonal structure is rather more active than flake-like structure for the photocatalytic NO oxidation reaction.

Generally, the range of conversion of all samples are in between 26% to 56%. Nevertheless, two samples from Group 1 which are AT 06 and AT 12 showed higher conversion values with 60% and 75% respectively. Among the samples only AT 06 and AT 12 have relatively closer reaction rate to that of the commercial TiO_2 photocatalyst. Both samples seem to have lower (002) intensity in their XRD patterns compared to other plane intensities. In addition to that both have hexagonal rod like structure.
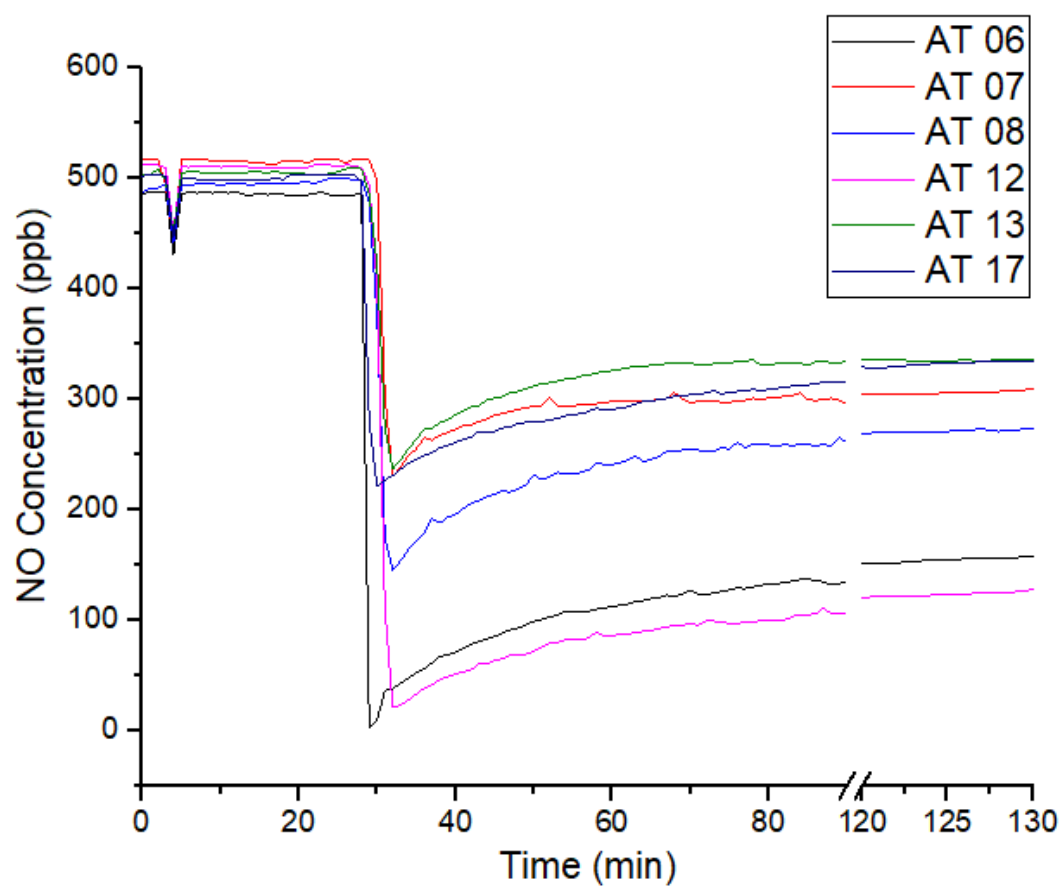
Figure 17: NO Oxidation Performance with ZnO Samples in Group 1
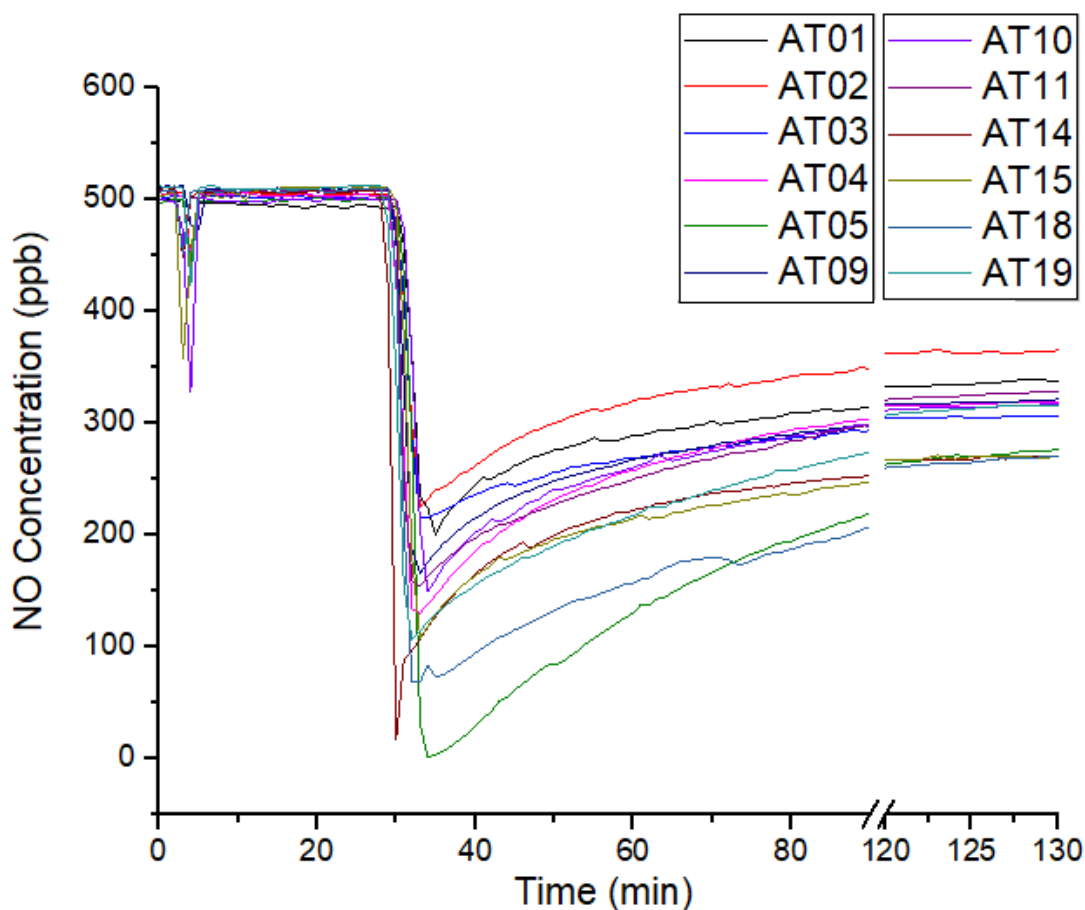
Figure 18: NO Oxidation Performance with ZnO Samples in Group 2

Looking at the Figure 16 and 17, the NO oxidation behavior of Group 1 and Group 2 ZnO samples can be investigated. For the Group 2 samples, generally longer times are needed to reach steady state. On the other hand, Group 1 samples reach steady state in less than 40 minutes once the UV irradiation starts. The reason why Group 1 samples reach steady state faster than Group 2 samples can be associated with the high stability in the Group 1 samples compared to the samples at Group 2.

Although AT 06 have a very small particle size, it shows the characteristic properties of the Group 1 samples at the XRD relative intensity ranking classification. The high

58

conversion at AT 06 can be associated with its high surface area with relatively more available adsorption sites. Besides, the number of all available planes increase when the surface area is very high. Therefore, potentially larger amount of planes can be present where the NO oxidation reaction is favored. On the other hand, AT 12 have particularly high particle size and a low BET surface area compared to most of the samples. Thus, the morphology of AT 12 can be worth to be investigated to understand and unravel the high conversion at its surface.

The high conversion at the AT 12 can be associated with its distinct morphology. As different from the other samples at Group 1, the AT 12 has shorter particles where the growth in (100) plane is dominant. At that particular morphology, that plane is expected to consist mostly Zn atoms connected to the subsurface oxygen atoms as different from other samples as shown in Figure 3. It can be said that the wide and open hexagonal structure can be more responsive to the NO oxidation reaction. As a result, increasing the relative area of the hexagon slices at the AT 12 structure can increase the NO oxidation reaction conversion. Among the samples, what can be concluded is that the AT 12 has the most appropriate orientation for this reaction, and further investigation of its distinct XRD relative intensity data can give information about the reaction active sites.

Table 7: Calculated NO Oxidation Rate Values for Each ZnO Sample

Group	Sample	BET (m^2/gram)	% NO Conversion	rNO(μmol/gcat.sec)
1	AT 07	5.73	39	2.32×10^{-3}
1	AT 12	4.3	75	4.46×10^{-3}
1	AT 08	1.22	50	2.98×10^{-3}
1	AT 13	1.06	34	2.02×10^{-3}
1	AT 17	3.65	30	1.79×10^{-3}
1	AT 06	12.5	60	3.57×10^{-3}
2	AT 02	11.1	26	1.55×10^{-3}
2	AT 03	9.73	40	2.38×10^{-3}
2	AT 04	10.0	39	2.32×10^{-3}
2	AT 05	8.74	36	2.14×10^{-3}
2	AT 01	8.26	32	1.90×10^{-3}
2	AT 09	14.6	35	2.08×10^{-3}
2	AT 14	15.2	27	1.61×10^{-3}
2	AT 18	10.5	56	3.33×10^{-3}
2	AT 19	11.7	42	2.50×10^{-3}
2	AT 10	15.65	41	2.44×10^{-3}
2	AT 15	14.90	48	2.86×10^{-3}
2	AT 11	13.85	38	2.26×10^{-3}
	Commercial TiO$_2$	47.0	88	5.24×10^{-3}

(*) % Conversion is recorded at the 90th minute of the NO oxidation experiment

This Page is Intentionally Left Blank

CHAPTER 5

CONCLUSIONS

NOx analysis test system based on ISO-22197:2007(E) standard was used to monitor the photocatalytic activity of ZnO nanoparticles through NO oxidation reaction.

19 different ZnO samples with different morphology, particle size and crystallinity were donated by Admire Tech Company. XRD analysis was used to determine the direction of the crystal growth of the ZnO particles and to reveal the dominant crystal orientation for each ZnO crystal structure. A simple classification of the samples were made depending on the rank of the plane indices from highest intensity to the lowest. Two groups are formed after the classification which are named as Group 1 and Group 2.

SEM imaging was performed to all samples to evaluate the morphology of the synthesized ZnO structures. The resulting images were found to be compatible with the findings of the XRD analysis.

Finally, the NO oxidation performance of each catalyst sample was determined using the ISO 22197-1 standard procedure. The NO conversion at the AT 12 and AT 06 showed the highest performance among all samples with a conversion of 75% and 60% respectively. The reason of this high conversion was attributed to the high activity of the 001 planes which were dominant in the best performing samples. It must be noted that the best performing ZnO samples exhibited NO oxidation rates (per gram catalyst basis) very close to that of commercial TiO_2 (Degussa P25) despite their surface areas were an order of magnitude smaller than TiO_2.

As the final remark it is said that the outcomes of the XRD analysis can reveal the major crystal orientations in the crystal structure and the NO oxidation method is used to find out the effect of this difference in morphologies. It is seen that the rate of photocatalytic NO oxidation reaction was higher at particular crystal planes.

This Page is Intentionally Left Blank

REFERENCES

[1]   J. A. Bernstein *et al.*, "The health effects of nonindustrial indoor air pollution," *J. Allergy Clin. Immunol.*, vol. 121, no. 3, pp. 585–591, 2008.

[2]   M. M. Ballari and H. J. H. Brouwers, "Full scale demonstration of air-purifying pavement," *J. Hazard. Mater.*, vol. 254–255, no. 1, pp. 406–414, 2013.

[3]   F. A. Cataño, S. H. Valencia, E. A. Hincapié, G. M. Restrepo, and J. M. Marín, "A Comparative study between TiO2and ZnO photocatalysis: Photocatalytic degradation of cibacron yellow FN-2R dye," *Lat. Am. Appl. Res.*, vol. 42, no. 1, pp. 33–38, 2012.

[4]   C. H. Ao, S. C. Lee, C. L. Mak, and L. Y. Chan, "Photodegradation of volatile organic compounds (VOCs) and NO for indoor air purification using TiO2: Promotion versus inhibition effect of NO," *Appl. Catal. B Environ.*, vol. 42, no. 2, pp. 119–129, 2003.

[5]   B. Han and L. Zhang, *Smart and multifunctional concrete toward sustainable infrastructures / Baoguo Han, Liqing Zhang, Jinping Ou*. Springer, 2017.

[6]   M. M. Ballari, M. Hunger, G. Hüsken, and H. J. H. Brouwers, "NOx photocatalytic degradation employing concrete pavement containing titanium dioxide," *Appl. Catal. B Environ.*, vol. 95, no. 3–4, pp. 245–254, 2010.

[7]   S. Shen, M. Burton, B. Jobson, and L. Haselbach, "Pervious concrete with titanium dioxide as a photocatalyst compound for a greener urban road environment," *Constr. Build. Mater.*, vol. 35, pp. 874–883, 2012.

[8]   K. Gopalakrishnan, J. Steyn, and J. Harvey, *Green Energy and Technology*

Climate Change, Energy, Sustainability and Pavements. 2014.

[9]   A. Beeldens, "Air Purification by Road Materials: Results of the Test Project in Antwerp," *Pap. Present. Int. RILEM Symp. Photocatal. . Environ. Constr. Mater.*, vol. TDP, 2007.

[10]   Essroc, "LEED-NC ® 2.2 Guide:Using TX Arca® and TX Aria®," *Photocatalytic Cem. New Constr. Major Renov. Nazareth, PA*, 2008.

[11]   Italcementi, "The Photocatalytic Active Principle: Technical Report," *TX Act. Bergamo Italy*, 2009.

[12]   J. Gignoux, L; Christory, J; Petit, "Concrete roadways and air quality -- Assessment of trials in Vanes in the hear of the Paris region," *Pap. Present. 12th Int. Symp. Concr. Raods, Sevilla, Spain*, 2010.

[13]   E. Beeldens, A; Boonen, "A double layered photocatalytic concrete pavement: a durable application with air-purifying properties," *Pap. Present. 10th Int. Conf. Concr. Pavements, Quebec City, Canada*, 2012.

[14]   A. Hassan, M, Okeil, "Field and Laboratory Investigation of Photocatalytic Pavements: Final Report," *Bat. Rouge, LA Gulf Coast Res. Cent. Evacuation Transp. Resiliency*, 2011.

[15]   Y. Ohama, *Application of Titanium Dioxide Photocatalysis to Construction Materials*. 2011.

[16]   S. Crispino, M; Vismara, "Innovative Photocatalytic Pavements Presentation," *Int. Sustain. Pavements Work. Airie, VA*, 2010.

[17]   T. P. Madsen *et al.*, "Field study of air purifying paving elements containing TiO 2," *Atmos. Environ.*, vol. 107, no. 2, pp. 44–51, 2015.

[18]   M. M. Khan, S. F. Adil, and A. Al-Mayouf, "Metal oxides as photocatalysts," *J. Saudi Chem. Soc.*, vol. 19, no. 5, pp. 462–464, 2015.

[19] S. G. Kumar and K. S. R. K. Rao, "Zinc oxide based photocatalysis: Tailoring surface-bulk structure and related interfacial charge carrier dynamics for better environmental applications," *RSC Adv.*, vol. 5, no. 5, pp. 3306–3351, 2015.

[20] J. Ungula and B. F. Dejene, "Effect of solvent medium on the structural, morphological and optical properties of ZnO nanoparticles synthesized by the sol-gel method," *Phys. B Condens. Matter*, vol. 480, pp. 26–30, 2016.

[21] A. Di Mauro, M. E. Fragalà, V. Privitera, and G. Impellizzeri, "ZnO for application in photocatalysis: From thin films to nanostructures," *Mater. Sci. Semicond. Process.*, vol. 69, no. July 2016, pp. 44–51, 2017.

[22] R. Qiu *et al.*, "Photocatalytic activity of polymer-modified ZnO under visible light irradiation," *J. Hazard. Mater.*, vol. 156, no. 1–3, pp. 80–85, 2008.

[23] A. Janotti and C. G. Van De Walle, "Fundamentals of zinc oxide as a semiconductor," *Reports Prog. Phys.*, vol. 72, no. 12, 2009.

[24] A. Kolodziejczak-Radzimska and T. Jesionowski, "Zinc oxide-from synthesis to application: A review," *Materials (Basel).*, vol. 7, no. 4, pp. 2833–2881, 2014.

[25] L. Lu, R. Li, C. Hu, Y. Xing, and Y. Zhu, "Morphological controlled preparation and photocatalytic activity of zinc oxide," *Mater. Chem. Phys.*, vol. 217, no. January, pp. 182–191, 2018.

[26] I. John Peter, E. Praveen, G. Vignesh, and P. Nithiananthi, "ZnO nanostructures with different morphology for enhanced photocatalytic activity," *Mater. Res. Express*, vol. 4, no. 12, 2017.

[27] "Fine ceramics (advanced ceramics, advanced technical ceramics) — Test method for air-purification performance of semiconducting photocatalytic materials," *ISO Int. Stand. 22197-1*, vol. 2004, 2004.

[28] N. Barbero and D. Vione, "Why Dyes Should Not Be Used to Test the

Photocatalytic Activity of Semiconductor Oxides," *Environ. Sci. Technol.*, vol. 50, no. 5, pp. 2130–2131, 2016.

[29] J. C. Colmenares and R. Luque, "Heterogeneous photocatalytic nanomaterials: Prospects and challenges in selective transformations of biomass-derived compounds," *Chem. Soc. Rev.*, vol. 43, no. 3, pp. 765–778, 2014.

[30] K. Hashimoto, H. Irie, and A. Fujishima, "TiO2 Photocatalysis: A Historical Overview and Future Prospects," *Jpn. J. Appl. Phys.*, vol. 44, no. 12, pp. 8269–8285, 2005.

[31] S. N. Frank and A. J. Bard, "Heterogeneous photocatalytic oxidation of cyanide and sulfite in aqueous solutions at semiconductor powders," *J. Phys. Chem.*, vol. 81, no. 15, pp. 1484–1488, 1977.

[32] M. R. Hoffmann, S. T. Martin, W. Choi, and D. W. Bahnemann, "Environmental Applications of Semiconductor Photocatalysis," *Chem. Rev.*, vol. 95, no. 1, pp. 69–96, 1995.

[33] M. A. Fox and M. T. Dulay, "Heterogeneous photocatalysis," *Chem. Rev.*, vol. 93, no. 1, pp. 341–357, Jan. 1993.

[34] J. Herrmann, "Heterogeneous photocatalysis: fundamentals and applications to the removal of various types of aqueous pollutants," *Catal. Today*, vol. 53, pp. 115–129, 1999.

[35] P. Kanhere and Z. Chen, "A review on visible light active perovskite-based photocatalysts," *Molecules*, vol. 19, no. 12, pp. 19995–20022, 2014.

[36] M. Gratzel, *Energy Resources Through Photochemistry and Catalysis*. Academic Press, 1983.

[37] G. . Allen, P. . Janes, J. . Nicholson, J. . Dalton, N. . Jones, and K. . Hallam, "Photocatalytic oxidation of NO x gases using TiO 2 : a surface spectroscopic approach," *Environ. Pollut.*, vol. 120, no. 2, pp. 415–422, 2003.

[38] D. Uner, M. M. Oymak, and B. Ipek, "CO2 utilisation by photocatalytic conversion to methane and methanol," *Int. J. Glob. Warm.*, vol. 3, no. 1/2, p. 142, 2011.

[39] V. J. Babu, S. Vempati, T. Uyar, and S. Ramakrishna, "Review of one-dimensional and two-dimensional nanostructured materials for hydrogen generation," *Phys. Chem. Chem. Phys.*, vol. 17, no. 5, pp. 2960–2986, 2015.

[40] Y. Park, S. H. Lee, S. O. Kang, and W. Choi, "Organic dye-sensitized TiO2 for the redox conversion of water pollutants under visible light," *Chem. Commun.*, vol. 46, no. 14, pp. 2477–2479, 2010.

[41] A. L. Linsebigler, G. Lu, and J. T. Yates, "Photocatalysis on TiO2 Surfaces: Principles, Mechanisms, and Selected Results," *Chem. Rev.*, vol. 95, no. 3, pp. 735–758, 1995.

[42] E. Luévano-Hipólito, A. Martínez-de la Cruz, and E. López Cuéllar, "Performance of ZnO synthesized by sol-gel as photocatalyst in the photooxidation reaction of NO," *Environ. Sci. Pollut. Res.*, vol. 24, no. 7, pp. 6361–6371, 2017.

[43] H. Morkoç and Ü. Özgür, *Zinc Oxide: Fundamentals, Materials and Device Technology*. 2009.

[44] R. J. Barnes, R. Molina, J. Xu, P. J. Dobson, and I. P. Thompson, "Comparison of TiO2and ZnO nanoparticles for photocatalytic degradation of methylene blue and the correlated inactivation of gram-positive and gram-negative bacteria," *J. Nanoparticle Res.*, vol. 15, no. 2, 2013.

[45] S. Liang, K. Xiao, Y. Mo, and X. Huang, "A novel ZnO nanoparticle blended polyvinylidene fluoride membrane for anti-irreversible fouling," *J. Memb. Sci.*, vol. 394–395, pp. 184–192, 2012.

[46] Ü. Özgür, V. Avrutin, and H. Morkoç, *Zinc Oxide Materials and Devices Grown by Molecular Beam Epitaxy*. 2018.

[47] F. Viñes, O. Lamiel-Garcia, F. Illas, and S. T. Bromley, "Size dependent structural and polymorphic transitions in ZnO: From nanocluster to bulk," *Nanoscale*, vol. 9, no. 28, pp. 10067–10074, 2017.

[48] K. M. Lee, C. W. Lai, K. S. Ngai, and J. C. Juan, "Recent developments of zinc oxide based photocatalyst in water treatment technology: A review," *Water Res.*, vol. 88, pp. 428–448, 2016.

[49] I. Stefaniuk, B. Cieniek, I. Rogalska, I. S. Virt, and A. Kosciak, "Magnetic Properties of ZnO:Co Layers Obtained by Pulsed Laser Deposition Method," *Mater. Sci. Pol.*, vol. 36, no. 3, pp. 439–444, 2018.

[50] C. Lizama, J. Freer, J. Baeza, and H. D. Mansilla, "Optimized photodegradation of reactive blue 19 on TiO2 and ZnO suspensions," *Catal. Today*, vol. 76, no. 2–4, pp. 235–246, 2002.

[51] S. Sakthivel, B. Neppolian, M. V. Shankar, B. Arabindoo, M. Palanichamy, and V. Murugesan, "Solar photocatalytic degradation of azo dye: Comparison of photocatalytic efficiency of ZnO and TiO2," *Sol. Energy Mater. Sol. Cells*, vol. 77, no. 1, pp. 65–82, 2003.

[52] C. A. K. Gouvêa, F. Wypych, S. G. Moraes, N. Durán, N. Nagata, and P. Peralta-Zamora, "Semiconductor-assisted photocatalytic degradation of reactive dyes in aqueous solution," *Chemosphere*, vol. 40, no. 4, pp. 433–440, 2000.

[53] J. Han, W. Qiu, and W. Gao, "Potential dissolution and photo-dissolution of ZnO thin films," *J. Hazard. Mater.*, vol. 178, no. 1–3, pp. 115–122, 2010.

[54] M. Samadi, M. Zirak, A. Naseri, E. Khorashadizade, and A. Z. Moshfegh, "Recent progress on doped ZnO nanostructures for visible-light photocatalysis," *Thin Solid Films*, vol. 605, pp. 2–19, 2016.

[55] M. A. Rauf and S. S. Ashraf, "Fundamental principles and application of heterogeneous photocatalytic degradation of dyes in solution," *Chem. Eng. J.*,

vol. 151, no. 1–3, pp. 10–18, 2009.

[56] D. Rajamanickam and M. Shanthi, "Photocatalytic degradation of an organic pollutant by zinc oxide – solar process," *Arab. J. Chem.*, vol. 9, pp. S1858–S1868, 2016.

[57] A. Mclaren, T. Valdes-Solis, G. Li, and S. C. Tsang, "Shape and Size Effect of ZnO nanocrystals on Photocatalytic Activity Supporting Information," *J. Am. Chem. Soc.*, no. 001, pp. 12540–12541, 2009.

[58] Y. Wang, X. Li, N. Wang, X. Quan, and Y. Chen, "Controllable synthesis of ZnO nanoflowers and their morphology-dependent photocatalytic activities," *Sep. Purif. Technol.*, vol. 62, no. 3, pp. 727–732, 2008.

[59] D. Li and H. Haneda, "Morphologies of zinc oxide particles and their effects on photocatalysis," *Chemosphere*, vol. 51, no. 2, pp. 129–137, 2003.

[60] C. B. Ong, L. Y. Ng, and A. W. Mohammad, "A review of ZnO nanoparticles as solar photocatalysts: Synthesis, mechanisms and applications," *Renew. Sustain. Energy Rev.*, vol. 81, no. July 2016, pp. 536–551, 2018.

[61] M. S. Mohajerani, A. Lak, and A. Simchi, "Effect of morphology on the solar photocatalytic behavior of ZnO nanostructures," *J. Alloys Compd.*, vol. 485, no. 1–2, pp. 616–620, 2009.

[62] K. A. Wong, S. M. Lam, and J. C. Sin, "Wet chemically synthesized ZnO structures for photodegradation of pre-treated palm oil mill effluent and antibacterial activity," *Ceram. Int.*, vol. 45, no. 2, pp. 1868–1880, 2019.

[63] A. V. Desai and M. A. Haque, "Mechanical properties of ZnO nanowires," *Sensors Actuators, A Phys.*, vol. 134, no. 1, pp. 169–176, 2007.

[64] E. S. Jang, J. H. Won, S. J. Hwang, and J. H. Choy, "Fine tuning of the face orientation of ZnO crystals to optimize their photocatalytic activity," *Adv. Mater.*, vol. 18, no. 24, pp. 3309–3312, 2006.

[65]   Y. Xue *et al.*, "Effect of aspect ratio and surface defects on the photocatalytic activity of ZnO nanorods," *Sci. Rep.*, vol. 4, no. 1, pp. 4–11, 2014.

[66]   P. Banerjee, S. Chakrabarti, S. Maitra, and B. K. Dutta, "Zinc oxide nanoparticles - Sonochemical synthesis, characterization and application for photoremediation of heavy metal," *Ultrason. Sonochem.*, vol. 19, no. 1, pp. 85–93, 2012.

[67]   M. Vafaee and M. S. Ghamsari, "Preparation and characterization of ZnO nanoparticles by a novel sol-gel route," *Mater. Lett.*, vol. 61, no. 14–15, pp. 3265–3268, 2007.

[68]   A. Šarić, G. Štefanić, G. Dražić, and M. Gotić, "Solvothermal synthesis of zinc oxide microspheres," *J. Alloys Compd.*, vol. 652, pp. 91–99, 2015.

[69]   P. Rai, W. K. Kwak, and Y. T. Yu, "Solvothermal synthesis of ZnO nanostructures and their morphology-dependent gas-sensing properties," *ACS Appl. Mater. Interfaces*, vol. 5, no. 8, pp. 3026–3032, 2013.

[70]   S. Kuriakose, N. Bhardwaj, J. Singh, B. Satpati, and S. Mohapatra, "Structural, optical and photocatalytic properties of flower-like ZnO nanostructures prepared by a facile wet chemical method," *Beilstein J. Nanotechnol.*, vol. 4, no. 1, pp. 763–770, 2013.

[71]   Y. Sun, L. Wang, X. Yu, and K. Chen, "Facile synthesis of flower-like 3D ZnO superstructures via solution route," *CrystEngComm*, vol. 14, no. 9, pp. 3199–3204, 2012.

[72]   A. B. Mohamad, M. S. Takriff, K. Sopian, M. M. Ba-Abbad, and A. A. H. Kadhum, "Optimization of process parameters using D-optimal design for synthesis of ZnO nanoparticles via sol–gel technique," *J. Ind. Eng. Chem.*, vol. 19, no. 1, pp. 99–105, 2012.

[73]   S. K. Lim, S. H. Hwang, S. Kim, and H. Park, "Preparation of ZnO nanorods by microemulsion synthesis and their application as a CO gas sensor," *Sensors*

Actuators, B Chem., vol. 160, no. 1, pp. 94–98, 2011.

[74] P. K. Samanta and S. Mishra, "Wet chemical growth and optical property of ZnO nanodiscs," *Optik (Stuttg).*, vol. 124, no. 17, pp. 2871–2873, 2013.

[75] N. Garino, M. Fontana, M. Laurenti, C. Gerbaldi, and S. Porro, "Zinc oxide nanostructures by chemical vapour deposition as anodes for Li-ion batteries," *J. Alloys Compd.*, vol. 640, pp. 321–326, 2015.

[76] S. Ghosh, D. Majumder, A. Sen, and S. Roy, "Facile sonochemical synthesis of zinc oxide nanoflakes at room temperature," *Mater. Lett.*, vol. 130, pp. 215–217, 2014.

[77] V. Anand and V. C. Srivastava, "Zinc oxide nanoparticles synthesis by electrochemical method: Optimization of parameters for maximization of productivity and characterization," *J. Alloys Compd.*, vol. 636, pp. 288–292, 2015.

[78] M. Hasanpoor, M. Aliofkhazraei, and H. Delavari, "Microwave assisted synthesis of Zinc oxide nanoparticles," *Procedia Mater. Sci.*, no. 11, pp. 320–325, 2015.

[79] J. Wu *et al.*, "Synthesis of hierarchically structured ZnO spheres by facile methods and their photocatalytic deNOx properties," *J. Hazard. Mater.*, vol. 248–249, pp. 202–210, 2013.

[80] T. Huang, Yunfang; Guo, Chongshen; Huang, Lijun; Dong, Qiang; Yin, Shu; Sato, "Photocatalytic oxidation of NOx gases using ZnO with superstructure by a low temperature soft solution process," *Int. J. Nanotechnol.*, vol. 10, pp. 30–37, 2013.

[81] E. Kowsari and B. Bazri, "Synthesis of rose-like ZnO hierarchical nanostructures in the presence of ionic liquid/Mg2+ for air purification and their shape-dependent photodegradation of SO2, NOx, and CO," *Appl. Catal. A Gen.*, vol. 475, no. x, pp. 325–334, 2014.

[82]   E. Kowsari and S. Abdpour, "In-situ functionalization of mesoporous hexagonal ZnO synthesized in task specific ionic liquid as a photocatalyst for elimination of SO2, NOx, and CO," *J. Solid State Chem.*, vol. 256, no. June, pp. 141–150, 2017.

[83]   E. Luévano-Hipólito and A. Martínez-de la Cruz, "Sol–gel synthesis and photocatalytic performance of ZnO toward oxidation reaction of NO," *Res. Chem. Intermed.*, vol. 42, no. 5, pp. 4879–4891, 2016.

[84]   M. Y. Nava Núñez and A. Martínez-de la Cruz, "Nitric oxide removal by action of ZnO photocatalyst hydrothermally synthesized in presence of EDTA," *Mater. Sci. Semicond. Process.*, vol. 81, no. October 2017, pp. 94–101, 2018.

[85]   X. Chen, H. Zhang, D. Zhang, Y. Miao, and G. Li, "Controllable synthesis of mesoporous multi-shelled ZnO microspheres as efficient photocatalysts for NO oxidation," *Appl. Surf. Sci.*, vol. 435, pp. 468–475, 2018.

[86]   I. Bayar, "Photocatalytic Oxidation of NOx over TiO2 Containing Cement Based Materials," *MS Thesis, Middle East Tech. Univ. Ankara, Turkey*, no. X, p. 84.

[87]   D. Uner, I. Bayar, and T. Tabari, "The influence of relative humidity on photocatalytic oxidation of nitric oxide (NO) over TiO2," *Appl. Surf. Sci.*, vol. 354, pp. 260–266, 2015.

[88]   I. Manual, "Thermo Scientific Model 42i Instruction Manual Chemiluminescence NO-NO2-NOx Analyzer Part Number 101350-00," no. 2, 2015.

[89]   H. Fan and X. Jia, "Selective detection of acetone and gasoline by temperature modulation in zinc oxide nanosheets sensors," *Solid State Ionics*, vol. 192, no. 1, pp. 688–692, 2011.

[90] K. A. Adegoke, M. Iqbal, H. Louis, S. U. Jan, M. Anam, and O. S. Bello, "Photocatalytic Conversion of CO2Using ZnOSemiconductor by Hydrothermal Method," *Pakistan J. Anal. Environ. Chem.*, vol. 19, no. 1, pp. 1–27, 2018.

APPENDIX A

Preliminary Calculations

For calculating the NO oxidation rate, finding $F_{NO.O}$ is necessary for the given experimental conditions.

$$1 \text{ ppm} = \frac{1 \text{ gas volume}}{10^6 \text{ balance air volume}}$$

$$1 \text{ ppm NO} = \frac{1 \text{ μL NO}}{1 \text{ L balance air}}$$

NO oxidation experiments are conducted with 500 ppb NO concentration at 1L/min flowrate. The density of NO is 1.34 g/L. Thus,

$$F_{NO,O} = 0.5 \left(\frac{\text{μL NO}}{1 \text{ L air}}\right) \times \left(\frac{1 \text{L air}}{60 \text{ sec}}\right) \times \left(\frac{1.34 \text{ g}}{1 \text{L}}\right) \times \left(\frac{1 \text{ L}}{10^6 \text{μL}}\right) \times \left(\frac{1 \text{ molNO}}{30 \text{ gNO}}\right)$$

$$= 3.72 \text{x} 10^{-10} \left(\frac{\text{mol}}{\text{sec}}\right)$$

$$F_{NO,O} = 3.72 \text{x} 10^{-4} \left(\frac{\text{μmol}}{\text{sec}}\right)$$

CSTR assumption is used for the design equation.

$$\frac{dNa}{dt} = FA_0 - FA + rAV$$

At steady state;

$$-rA = \frac{(FA_0 \text{ X})}{V}$$

Per gram catalyst basis;

$$-rA = \frac{(FA_0 \text{ X})}{W}$$

Surface Average Particle Size Calculation with BET Area

Bulk density of ZnO is taken as 8.81×10^5 g/m^3

$$D_{surface} = \frac{6}{\rho \text{ x BET area}}$$

Volume Average Particle Size Calculation with Scherrer Equation

$$D_{volume} = \frac{k\lambda}{\beta \cos\theta}$$

Where the variables are defined as;

D= Average particle size

B= Peak broadening of the highest peak in radiant (corresponds to FWHM of the peak under certain assumptions)

λ = Cu K-α wavelength (0.15418 nm)

θ= Half of the Bragg angle

k= Constant (0.94)

APPENDIX B

ZnO Synthesis Methodology

The method is developed at Admire Tech Company by Dr. Ertuğrul Erkoç. The chemical reagents zinc acetate dehydrate $(Zn(CH_3CO_2)_2).H_2O$ DEQ (98%) and sodium hydroxide (NaOH, DEQ. (98%)) were used for the preparation of the ZnO samples.

The synthesis of ZnO was performed by using T type minireactor. Initially 0.125 M Zinc Acetate and 0.25 M Sodium Hydroxide solutions are prepared. Then a solution is obtained by mixing zinc acetate (ZnAc) and sodium hydroxide (NaOH) by mixing in T type minireactor in different amounts to give molar ratios of NaOH/ZnAc: 1, 1.5, 2, 2.5, 2.76, 3 and 3.5. The resulting white precipitate are filtered, washed three times with hot deionized water and dried at 70 °C for overnight. ZnO samples are grouped with respect to their NaOH/ZnAc reaction stoichiometry. The synthesized ZnO samples are labeled as it is indicated at Table B.1. The samples with the same synthesis stoichiometry differs in their flow regime during the reaction in the minireactor.

Table B.1: The Reaction Stoichiometries of the ZnO Samples Produced at the Synthesis

NaOH:ZnAc	Samples (AT)
1:1	07,12,16
1.5:1	08,13,17
2:1	01,02,03,04,05,06
2.5:1	09,14,18
2.76:1	19
3:1	10,15
3.5:1	11

APPENDIX C

NOx Photoreactor

Figure C.1: Plexiglass NOx Photoreactor used in the NO Oxidation Experiment

This Page is Intentionally Left Blank